Available online at www.sciencedirect.com
ScienceDirect
Geochimica et Cosmochimica Acta 74 (2010) 6610–6635
Geochimica et Cosmochimica Acta
www.elsevier.com/locate/gca

High precision SIMS oxygen three isotope study of chondrules in LL3 chondrites: Role of ambient gas during chondrule formation

Noriko T. Kita [a,*], Hiroko Nagahara [b], Shogo Tachibana [b], Shin Tomomura [b], Michael J. Spicuzza [a], John H. Fournelle [a], John W. Valley [a]

[a] WiscSIMS, Department of Geoscience, University of Wisconsin-Madison, 1215 W. Dayton St., Madison, WI 53706, USA
[b] Department of Earth and Planetary Science, University of Tokyo, 7-3-1 Hongo, Tokyo 113-0033, Japan

Received 3 September 2009; accepted in revised form 9 August 2010; available online 14 August 2010

Abstract

We report high precision SIMS oxygen three isotope analyses of 36 chondrules from some of the least equilibrated LL3 chondrites, and find systematic variations in oxygen isotope ratios with chondrule types. FeO-poor (type I) chondrules generally plot along a mass dependent fractionation line ($\Delta^{17}O \sim 0.7‰$), with $\delta^{18}O$ values lower in olivine-rich (IA) than pyroxene-rich (IB) chondrules. Data from FeO-rich (type II) chondrules show a limited range of $\delta^{18}O$ and $\delta^{17}O$ values at $\delta^{18}O = 4.5‰$, $\delta^{17}O = 2.9‰$, and $\Delta^{17}O = 0.5‰$, which is slightly ^{16}O-enriched relative to bulk LL chondrites ($\Delta^{17}O \sim 1.3‰$). Data from four chondrules show ^{16}O-rich oxygen isotope ratios that plot near the CCAM (Carbonaceous Chondrite Anhydrous Mineral) line. Glass analyses in selected chondrules are systematically higher than co-existing minerals in both $\delta^{18}O$ and $\Delta^{17}O$ values, whereas high-Ca pyroxene data in the same chondrule are similar to those in olivine and pyroxene phenocrysts.

Our results suggest that the LL chondrite chondrule-forming region contained two kinds of solid precursors, (1) ^{16}O-poor precursors with $\Delta^{17}O > 1.6‰$ and (2) ^{16}O-rich solid precursors derived from the same oxygen isotope reservoir as carbonaceous chondrites. Oxygen isotopes exhibited open system behavior during chondrule formation, and the interaction between the solid and ambient gas might occur as described in the following model. Significant evaporation and recondensation of solid precursors caused a large mass-dependent fractionation due to either kinetic or equilibrium isotope exchange between gas and solid to form type IA chondrules with higher bulk Mg/Si ratios. Type II chondrules formed under elevated dust/gas ratios and with water ice in the precursors, in which the ambient H_2O gas homogenized chondrule melts by isotope exchange. Low temperature oxygen isotope exchange may have occurred between chondrule glasses and aqueous fluids with high $\Delta^{17}O$ ($\sim 5‰$) in LL the parent body. According to our model, oxygen isotope ratios of chondrules were strongly influenced by the local solid precursors in the proto-planetary disk and the ambient gas during chondrule melting events.

1. INTRODUCTION

Petrographic, chemical, and isotopic studies of chondrules from primitive meteorites indicate their formation by transient heating of dust aggregates in the protoplanetary disk (e.g., Grossman, 1988; Jones et al., 2005), though the details of chondrule formation are controversial (e.g., Ciesla, 2005). Among the many proposed mechanisms of chondrule-forming heating events, shock wave heating in the proto-planetary disk is considered to be most promising and explains many properties of chondrules (Connolly and Love, 1998). It has been suggested that chondrule-forming melting events occurred in an environment significantly enriched in dust compared to the average solar gas based on the volatile element abundance (e.g., Lewis et al., 1993; Nagahara et al., 1994), absence of isotopic mass fractionation of K and Fe

* Corresponding author. Tel.: +1 608 262 7118.
E-mail address: noriko@geology.wisc.edu (N.T. Kita).

0016-7037/$ - see front matter © 2010 Elsevier Ltd. All rights reserved.
doi:10.1016/j.gca.2010.08.011

(Alexander et al., 2000; Alexander and Wang, 2001; Alexander and Grossman, 2005) and Na concentrations (Alexander et al., 2008). Recent studies also suggest that some chondrules formed in an open system involving evaporation and recondensation of alkali elements and Si (Tissandier et al., 2002; Krot et al., 2004; Libourel et al., 2006; Nagahara et al., 2008). However, zonation of alkali elements observed in at least some chondrules may be caused by elemental exchange at low temperature in the parent body (Grossman et al., 2002; Alexander and Grossman, 2005).

Oxygen isotope ratios in the early solar system are considered to be significantly heterogeneous in ^{16}O, based on the analyses of Ca, Al-rich inclusions (CAIs), chondrules, and matrix minerals (e.g., Clayton et al., 1973, 1977; Clayton, 1993; Yurimoto and Wasson, 2002; Jones et al., 2004; Kobayashi et al., 2003; Sakamoto et al., 2007). The variations of $^{18}O/^{16}O$ and $^{17}O/^{16}O$ ratios in meteorites, which are expressed as $\delta^{18}O$ and $\delta^{17}O$, permil (‰) deviation from SMOW (Standard Mean Ocean Water), respectively, range from −80‰ in a rare cryptocrystalline chondrule in CH chondrite Acfer 214 (Kobayashi et al., 2003) to +200‰ in a sulfide-rich matrix assemblage from Acfer 094 ungrouped carbonaceous chondrite (Sakamoto et al., 2007).

The oxygen isotope ratios of CAIs, the oldest solids in the solar system (Amelin et al., 2002), are uniformly ^{16}O-rich by 50–60‰ (e.g., McKeegan et al., 1998; Hiyagon and Hashimoto, 1999; Guan et al., 2000; Gounelle et al., 2009; Makide et al., 2009) and similar to the analyses of solar wind from Genesis samples (McKeegan et al., 2010). It has been suggested that the mass independent fractionation of a CO molecule by photochemical reaction might produce large enrichments of ^{17}O and ^{18}O as a form of water or ice, either in the molecular cloud or in the protoplanetary disk (e.g., Thiemens and Heidenreich, 1983; Clayton, 2002; Yurimoto and Kuramoto, 2004; Lyons and Young, 2005). The highest $\delta^{18}O$ and $\delta^{17}O$ values observed from the matrix sulfide in Acfer 094 ungrouped carbonaceous chondrite may represent the extremely ^{16}O depleted water component (Sakamoto et al., 2007). Subsequent thermal processing of dust (e.g., during chondrule formation) in an ^{16}O-depleted gaseous reservoir resulted in evolution of O-isotope compositions of solids towards the terrestrial fractionation line. Alternatively, other models hypothesize the presence of distinct oxygen isotope reservoirs (^{16}O-rich gas and ^{16}O-poor solids) at the birth of the solar system (Gaidos et al., 2009; Krot et al., 2010). In contrast, chondrules are generally ^{16}O depleted compared to CAIs and show a significant variation in $\delta^{18}O$ and $\delta^{17}O$ values more than 10‰ among chondrules from different groups of chondrites (e.g., Clayton, 1993; Krot et al., 2006, 2009 and reference therein). Chondrules from least metamorphosed LL and CO chondrites do not show distinguishable ^{26}Al-relative ages (e.g., Kita et al., 2000; 2005; Kurahashi et al., 2008). These data suggest that oxygen isotope ratios in the protoplanetary disk were spatially heterogeneous at ~2 My after CAI formation (Kurahashi et al., 2008; Krot et al., 2009).

The distribution of oxygen three isotopes in chondrules at the μm scale may provide important insights into the process of isotope exchange between chondrule melt and surrounding gas (e.g., Yu et al., 1995; Boesenberg et al., 2005). Secondary ion mass spectrometer (SIMS, or ion microprobe) analyses of chondrules in carbonaceous chondrites show the existence of ^{16}O-rich relict olivine grains (Yurimoto and Wasson, 2002; Jones et al., 2004; Kunihiro et al., 2004, 2005). Chaussidon et al. (2008) reported detailed SIMS analyses of olivine, pyroxene, and mesostasis in chondrules in CV and CR chondrites. They argue that the oxygen isotope ratios in chondrules resulted from the interaction between precursor olivine grains with variable oxygen isotope ratios and SiO molecules in the nebular gas with specific isotope ratios. SIMS analyses of chondrules from unequilibrated ordinary chondrites (UOCs) are scarce due to the limited variation (~a few ‰), which was previously difficult to resolve by SIMS, as suggested by analysis of bulk chondrules (Clayton et al., 1991). Exceptions are the SIMS analyses of rare Al-rich chondrules in UOCs that are enriched in ^{16}O relative to ferromagnesian chondrules (Russell et al., 2000). Low density fractions from chondrules in UOCs, which concentrate glass and feldspar in chondrules, were analyzed by conventional gas-source mass spectrometers and show a significant depletion of ^{16}O by more than a few ‰ (Mayeda et al., 1989; Bridges et al., 1999), indicating that chondrules in UOCs could be internally zoned in oxygen three isotope ratios. In order to explore the potential for oxygen isotope zonation and resolve the origin of heterogeneity among chondrules in UOCs, we report the results of in-situ oxygen isotope analyses of UOC chondrules using a new generation SIMS, IMS-1280 at the WiscSIMS (Wisconsin secondary ion mass spectrometer) Laboratory, University of Wisconsin-Madison (Kita et al., 2009a; Valley and Kita, 2009). The new analytical protocols established at WiscSIMS are capable of obtaining oxygen three isotope ratios with high precision (±0.3–1‰, 2SD) and high spatial resolution (5–10 μm), which provides significantly improved analytical data compared with previous studies.

1.1. Oxygen three isotopes in chondrules from UOCs

Bulk oxygen isotope ratios of chondrules in ordinary chondrites plot slightly above the TF (terrestrial fractionation) line, showing a cluster of data around that of bulk ordinary chondrites (Fig. 1). They plot on the extension of the Young and Russell (Y&R) line derived from the in-situ laser fluorination analysis of unaltered CAI minerals (Young and Russell, 1998). In contrast, oxygen isotope ratios of chondrules in carbonaceous chondrites plot along the CCAM (Carbonaceous Chondrite Anhydrous Mineral) line, which is derived from regression of CAI mineral separates in CV3 chondrites (Clayton et al., 1977). The slope of the trend among OC chondrules is ~0.7, significantly flatter than that of the CV3 chondrule trend, indicating that mass dependent fractionation effects might exist among OC chondrules in addition to mass independent effects. Clayton et al. (1991) reported that there is no systematic correlation of oxygen isotope ratios with chondrule texture. Although bulk H, L and LL chondrites plot on different mass fractionation lines with $\Delta^{17}O$ ($= \delta^{17}O - 0.52 \times \delta^{18}O$) of 0.73 ± 0.18‰, 1.07 ± 0.18‰, 1.26 ± 0.24‰, respectively, the $\Delta^{17}O$ values of chondrules from H3, L3, and LL3

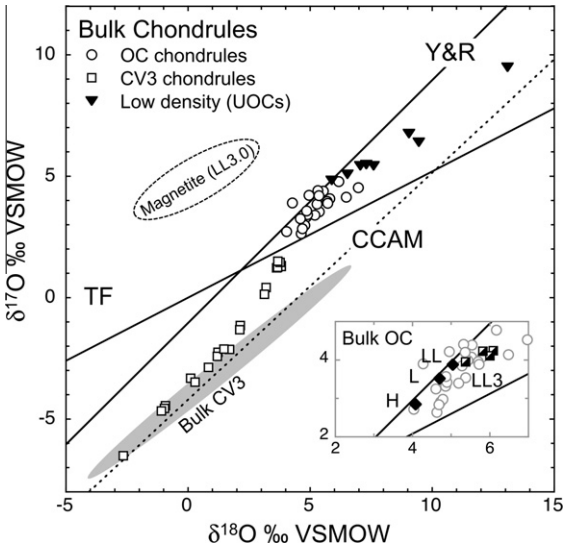

Fig. 1. The oxygen isotope ratios in chondrules from unequilibrated ordinary chondrites (UOCs) and bulk chondrules from Allende (CV3) chondrite from literature. The isotope ratios are expressed as $\delta^{18}O$ and $\delta^{17}O$ on the VSMOW scale. Terrestrial fractionation line ($\delta^{17}O = 0.52 \times \delta^{18}O$; TF) is shown as reference. Individual bulk chondrule data from UOCs and Allende (CV3) are shown as open circles and squares (Clayton et al., 1983, 1991). Similar results are obtained for UOC and CV3 chondrites by Bridges et al. (1998) and Jones et al. (2004), respectively. Low-density mineral separates (specific gravity <2.8) from UOCs are shown as filled triangles, which represent chondrule mesostasis (Bridges et al., 1999). The magnetite data from Semarkona (LL3.0) matrix with high $\Delta^{17}O \sim 5‰$ (Choi et al., 1998) and estimated range of aqueous fluid (assuming equilibrium fractionation factor of −11‰ between magnetite and aqueous fluid) are shown by oval areas. The average values of bulk types 4–6 H, L, LL chondrites (equilibrated ordinary chondrites, EOCs) are shown in the insert (Clayton et al., 1991), which plot along the Young and Russell (Y&R) line. The LL3 chondrite bulk analyses are shown as half filled squares that deviate slightly from LL4–6 average values (Clayton et al., 1991), most likely due to aqueous alteration of matrix minerals. Bulk CV3 chondrite data (grey hatched area; data from Clayton and Mayeda, 1999) plot nearly on the CCAM line.

chondrites are distributed randomly from 0.2‰ to 1.7‰ without systematic differences (Clayton et al., 1991).

The SIMS oxygen three isotope analyses of rare Al-rich chondrules in UOCs (Russell et al., 2000) show an enrichment of ^{16}O by more than 10‰, similar to the range of chondrules in carbonaceous chondrites. Feldspar and glass-rich separates of unequilibrated ordinary chondrites (UOC) are significantly higher in both $\delta^{18}O$ and $\delta^{17}O$ than bulk chondrules (Mayeda et al., 1989; Bridges et al., 1999, see Fig. 1), and extend the trend of bulk chondrules with a slope of ~0.7. These data indicate that individual chondrules could be internally heterogeneous in oxygen three isotopes. Analogous to chondrules from CV and CR chondrites discussed by Chaussidon et al. (2008), the oxygen isotope heterogeneity among UOC chondrules could be caused by gas–solid exchange in the solar nebula, in which case chondrule glass might record the ^{16}O-poor solar nebula gas. Alternatively, secondary processes in the parent body might affect oxygen isotope ratios in UOC chondrules. A similar process was suggested for the oxygen isotope ratios of mesostasis of Allende carbonaceous chondrite (Maruyama et al., 1999; Maruyama and Yurimoto, 2003). Choi et al. (1998) reported that ^{16}O-poor magnetite ($\Delta^{17}O \sim 5‰$) in Semarkona (subtype 3.0, LL3 chondrite) formed by aqueous alteration, indicating existence of ^{16}O-poor water in the parent body of ordinary chondrites. Aqueous alteration has affected some chondrule glass even in the least equilibrated subtypes (Grossman et al., 2000, 2002; Grossman and Brearley, 2005). The high precision SIMS analyses of $\delta^{18}O$ in chondrule glass may test whether oxygen isotopes in glass preserved the primary isotope ratios in chondrule melt that were equilibrated with nebula gas at high temperature, or they were altered by isotope exchange with aqueous fluid at low temperature, in which a significant heavy isotope enrichment (higher $\delta^{18}O$ values) could be observed.

2. ANALYTICAL PROCEDURES

2.1. Sample selection

Among the various chondrite groups, chondrules from UOC (type 3.0–3.9) have been studied in great detail and are considered to best preserve the original textural, chemical, and isotopic signature at the time of chondrule formation (Grossman and Wasson, 1983, 1987; Jones and Scott, 1989; Jones, 1990, 1994, 1996). We used three polished thin sections of UOCs with low subtypes (⩽3.2), Semarkona (LL3.0; USNM 1805-9, National Museum of Natural History at Smithsonian Institution), Bishunpur and Krymka (LL3.1; M3816 and L3802, respectively, Natural History Museum, Vienna). A more recent classification for low petrologic subtypes by Grossman and Brearley (2005) indicates Bishunpur (3.15) and Krymka (3.2) are more metamorphosed than Semarkona (3.00). We selected 12 chondrules from a thin section of Semarkona that include 5 chondrules previously studied for Al–Mg chronology (Kita et al., 2000; Tachibana et al., 2003) and one Al-rich chondrule that had been analyzed for mineralogy, and elemental and stable isotope compositions (Nagahara et al., 2008). For the Bishunpur and Krymka sections, a total of 86 chondrules were randomly selected and examined for their petrography, mineral chemistry, and bulk chemical compositions. From these chondrules, 14 from Bishunpur and 7 from Krymka were chosen for oxygen isotope analysis, which include 5 chondrules studied previously for Al–Mg chronology (Mostefaoui et al., 2002; Tachibana et al., 2003; Kita et al., 2005). Unfortunately, the Bishunpur and Krymka thin sections contain fusion crusts, and we avoided any samples within 1 mm of the fusion crusts for isotope analyses. Furthermore, both thin sections showed some polishing relief at the edge of the meteorite specimen; chondrules located at the edge of the specimens were not selected because of possible analytical artifacts from sample surface topography (Kita et al., 2009a).

Nagahara et al. (2008) reported oxygen and Mg isotope ratios in the Al-rich chondrule CH5 in Semarkona using the IMS-1270. The Mg isotope ratios in forsterite did not show

any resolvable mass fractionation (analytical uncertainty ~1‰, 2SD). However, the oxygen isotope ratios in CH5 show a mass-dependent fractionation in $\delta^{18}O$ that is lower than bulk ordinary chondrites by 2‰. This same chondrule was analyzed in our study with better precision and accuracy to confirm the previous results.

2.2. Electron microprobe analyses

Prior to oxygen isotope analysis, individual chondrules were examined using scanning electron microscopes (SEM), JEOL JSM-7000F at the University of Tokyo and Hitachi S-3400 at the University of Wisconsin-Madison. For some chondrules containing forsteritic olivine, cathodoluminescence (CL) images were also obtained using CL detectors on the S-3400 with three color filters (RGB). Bulk chemical compositions of 86 chondrules from Bishunpur and Krymka were obtained by using a JEOL JXA-8900 electron microprobe at the University of Tokyo with the method described in Tachibana et al. (2003). For some chondrules analyzed by SIMS, major element compositions of olivine, pyroxene, and glass were obtained with a CAMECA SX51 electron microprobe at the University of Wisconsin (an accelerating voltage of 15 kV with a focused beam of 12 nA for olivine and pyroxene and defocused beam (5 μm) of 3 nA for glass using synthetic and natural analytical standards), and also with an EDS X-ray detector equipped on the JEOL JSM-7000F for olivine and pyroxene. After SIMS analysis, all SIMS pits were inspected by Hitachi S-3400 SEM to confirm the positions of analyses, and to inspect for possible irregularities in the samples, such as unseen inclusions or cracks.

2.3. SIMS oxygen three isotope analysis

We used a large radius SIMS, CAMECA IMS-1280 for in-situ oxygen isotope analyses. We have developed a protocol for highly precise and accurate oxygen three isotope analyses using multi-collection Faraday Cup (FC) detectors. The analytical conditions are generally similar to those of Kita et al. (2004) using an IMS-1270, although the new software and additional hardware of the IMS-1280 resulted in faster, more precise, and more accurate stable isotope analyses (e.g., Downes et al., 2008; Nakamura et al., 2008; Kita et al., 2009a; Valley and Kita, 2009). More descriptions of analytical and sample preparation protocols using the WiscSIMS IMS-1280 can be found in Kita et al. (2009a). The chondrule analyses were made in three separate sessions (S1, S2, and S3) with slightly different analytical conditions. We used a focused Cs^+ primary beam (Gaussian mode) with ion currents of 3.5 nA (S1 and S2) and 0.5 nA (S3), and beam spot diameters of 15 and 5 μm, respectively. The normal incidence electron gun was used for charge compensation. Intensities of ^{16}O were 3×10^9 and 4×10^8 counts per second (cps) for the 15 and 5 μm primary beam conditions, respectively. Both ^{17}O and ^{18}O signals were higher than 10^6 cps for sessions with 15 μm spots (S1 and S2), so that all three isotopes were simultaneously measured with FC detectors. In the session with 5 μm spots (S3), ^{17}O signals were measured with an electron multiplier (EM) detector in pulse counting mode. The mass resolving power (MRP) was set to ~2200 for ^{16}O and ^{18}O using two detectors on the multi-collection array, and 4500 for ^{17}O using the axial detector (sometimes called the "mono-collector" with fixed position). The correction for OH^- interference on ^{17}O was checked for each analysis and found to be negligibly small (<0.1‰) except for a few cases. Detailed analytical parameters are described in EA1 and listed in Table EA2-1.

A thin section of a San Carlos (SC) olivine standard (Fo_{89}; $\delta^{18}O = 5.32$‰ VSMOW, see Table EA2-2) was used as the running standard during the chondrule analyses and each series of 10–25 sample analyses are bracketed by 8–10 analyses of SC olivine (Kita et al., 2009a). External reproducibility of bracket standard analyses is calculated as twice the standard deviation (2SD) of ~8 spots and were typically 0.3‰ for $\delta^{18}O$ and 0.3–1‰ for $\delta^{17}O$ and $\Delta^{17}O$, during the 15 μm spot analyses (S1 and S2), and ⩽1‰ for all ratios during the 5 μm spot analyses (S3). The external reproducibility of $\delta^{17}O$ is similar to the internal error of a single analysis, which is consistent with FC detector thermal noise (~2000 cps in 4 s integration; S1 and S2) or counting statistics of total number of ions detected (S3). However, the external reproducibility of $\delta^{18}O$ is worse than the internal error of a single analysis, indicating that the instrumental bias changes slightly from spot to spot (Kita et al., 2009a). Thus, 2SD values of bracketing standard analyses represent spot-to-spot reproducibility and were assigned as the uncertainties of the individual spot analyses.

To obtain accurate $\delta^{18}O$ and $\delta^{17}O$ data, SIMS instrumental bias should be corrected properly using appropriate standards with homogeneous oxygen isotope ratios and matching chemical compositions and crystal structure. For this purpose, we used a series of olivine and pyroxene standards, the ranges of Fo_{100}–Fo_{60} for olivine, and En_{97}–En_{85} and Wo_0–Wo_{50} for pyroxene, which are similar to the range of olivine and pyroxene compositions found in chondrules. Several olivine and pyroxene standards were analyzed in this work using laser fluorination and a gas-source mass spectrometer at the University of Wisconsin (Valley et al., 1995). The results of analyses are shown in Table EA2-2. The instrumental biases for $\delta^{18}O$ from olivine and pyroxene standards with similar major element compositions are reproducible at the level of 0.2–0.4‰ (Table EA2-3; in S4 and S5). For the analysis of glass, we used a set of glass standards with known $\delta^{18}O$ values from Max-Planck Institute (MPI-DING glass, Jochum et al., 2006) that cover the range of SiO_2 contents from 50% (basalt) to 76% (rhyolite). The major element compositions of these standards are generally similar to compositions of chondrule glass except chondrule glass shows a wider range of FeO content. These standards are listed in Table EA2-2 and bias correction procedures are described in EA1. The raw SIMS data for these standards are listed in Tables EA3-1 and EA3-2.

It is generally expected that the average value of multiple analyses from homogeneous samples will be determined with a higher precision, because the error estimated for the average value is reduced by inverse of square root of number of analyses. However, the accuracy of in-situ SIMS

measurements of $\delta^{18}O$ values are usually limited at the level of 0.3‰ with the following reasons. First, instrumental biases obtained from olivine and pyroxene standards are reproducible at the level of ~0.3‰ in $\delta^{18}O$, even between standards with very similar major element compositions (Table EA2-3). Second, a small polishing relief of meteorite samples or the position of sample on the SIMS sample stage may cause a small instrumental bias in $\delta^{18}O$ at the level of 0.3‰ (Kita et al., 2009a). It is not easy to estimate changes in the instrumental biases at the level of 0.1‰ that are caused by subtle differences in the condition of samples and the instrument. Therefore, in this study, the uncertainty of 0.3‰ in $\delta^{18}O$ is propagated to those of the average values of multiple analyses. By assuming that the SIMS instrumental bias is mass dependent for oxygen isotopes, the uncertainty of $\delta^{17}O$ at the level of 0.15‰ (i.e., a half of those of $\delta^{18}O$ because $^{18}O/^{16}O$ ratios changes twice as the $^{17}O/^{16}O$ ratios) is propagated to the average value of the multiple spots. For the same reason, mass fractionation corrected $\Delta^{17}O$ values are insensitive to these small instrumental biases. Indeed, the ultimate precision and accuracy of $\Delta^{17}O$ measurement were found to be as good as 0.1‰ in our previous studies (e.g., Kita et al., 2009b; Heck et al., 2010).

3. RESULTS

3.1. Petrography and chemistry of chondrules

The mineralogy and bulk major element compositions of randomly selected chondrules from Bishunpur and Krymka are summarized in Table EA4. They are dominated by porphyritic textures (74 chondrules, 86%) that are classified by mg# (molar % [MgO]/[MgO + FeO]) into type I (FeO-poor; mg# ⩾ 90) and type II (FeO-rich; mg# < 90). They are further divided by the proportion of olivine and pyroxene; type A (>80% olivine), type AB (20–80% olivine) and type B (<20% olivine). The texture and mineral chemistry of the porphyritic ferromagnesian chondrules studied here are similar to those described in a series of papers by Jones and her coauthors on ferromagnesian chondrules in Semarkona and other unequilibrated LL3 chondrites (Jones and Scott, 1989; Jones, 1990, 1994, 1996). In addition to porphyritic ferromagnesian chondrules, there are 8 radial pyroxene chondrules (9.3%), 1 barred olivine chondrule (1%) and 3 Al-rich chondrules (3%).

The average bulk-silicate major-element compositions are calculated for different chondrule types using 86 chondrules in Bishunpur and Krymka studied in this work and an additional 6 Semarkona chondrules from Tachibana et al. (2003) and Nagahara et al. (2008). The results are shown in Table 1, and selected elements are shown in CI normalized abundance in Fig. 2. The 36 chondrules selected for oxygen isotope analysis are listed in Table EA5: one Al-rich chondrule, 17 type I chondrules, 16 type II chondrules and 2 radial pyroxene (RP) chondrules. The proportion of chondrule types is generally consistent with that of randomly selected chondrules (Table EA4). Therefore, our oxygen isotope data set likely represents the main population of ferromagnesian chondrules in LL3.0–3.1 chondrites.

The BSE images of selected chondrules are shown in Fig. 3. EPMA analyses of olivine, pyroxene, and glass for these chondrules are listed in Table EA6. The CL images of five type I chondrules (CH5, CH33, CH44, CH61, and B3) are examined because they contain olivine with nearly pure forsterite (⩾Fo_{99}). Type IA chondrules CH44 and

Table 1
Average bulk silicate major element compositions (wt%)[a] and CI normalized (Mg/Si) ratios of chondrules in LL3 chondrites.

Type		n[b]	SiO_2	TiO_2	Al_2O_3	Cr_2O_3	FeO	MnO	MgO	CaO	Na_2O	K_2O	Total	$(Mg/Si)_{CI}$
Al-rich[c]		3	47.12	0.82	17.43	0.23	0.75	0.08	18.34	13.99	0.49	0.02	99.26	0.54
	1SD		2.19	0.04	1.01	0.09	0.31	0.01	2.54	0.92	0.49	0.01		
IA		9	44.24	0.15	3.04	0.41	4.62	0.20	43.98	2.08	0.65	0.07	99.44	1.38
	1SD		1.95	0.07	1.42	0.12	2.51	0.20	4.15	1.04	0.46	0.06		
IAB		22	49.29	0.15	2.74	0.63	5.04	0.30	38.70	2.08	0.54	0.07	99.54	1.09
	1SD		2.84	0.04	0.81	0.14	1.60	0.13	3.46	0.67	0.29	0.07		
IB		13	54.43	0.14	2.49	0.64	4.35	0.37	34.55	1.76	0.55	0.06	99.34	0.88
	1SD		1.14	0.03	0.91	0.08	1.26	0.13	2.41	0.48	0.35	0.04		
IIA		12	46.82	0.13	2.33	0.50	13.58	0.46	32.47	1.96	0.99	0.19	99.42	0.96
	1SD		3.75	0.05	1.11	0.13	3.97	0.08	4.92	0.88	0.42	0.11		
IIAB		14	47.02	0.12	1.97	0.64	15.27	0.52	30.35	2.11	0.74	0.10	98.84	0.90
	1SD		2.63	0.02	0.49	0.07	3.79	0.08	2.75	0.33	0.37	0.07		
IIB		5	53.34	0.09	1.52	0.68	10.39	0.46	31.23	1.47	0.34	0.02	99.55	0.81
	1SD		2.29	0.02	0.52	0.07	3.86	0.10	2.88	0.37	0.20	0.01		
II-Plag[d]		4	42.39	0.13	2.88	0.64	14.99	0.27	34.91	2.47	0.12	0.02	98.84	1.14
	1SD		1.61	0.02	0.76	0.07	2.22	0.04	2.05	0.33	0.07	0.01		
BO		1	45.87	0.13	1.88	0.59	20.38	0.57	26.64	2.09	0.73	0.17	99.05	0.81
RP (FeO-poor)		2	54.92	0.32	6.23	0.59	1.84	0.23	29.85	4.12	1.32	0.07	99.47	0.75
	1SD		3.04	0.11	2.77	0.15	0.39	0.13	3.44	1.50	0.64	0.02		
RP (FeO-rich)		6	54.13	0.10	1.68	0.77	12.31	0.67	27.77	1.50	0.52	0.06	99.51	0.71
	1SD		2.52	0.02	0.42	0.12	3.82	0.14	2.41	0.44	0.32	0.03		

[a] The average values are calculated from EPMA data in EA4 and EA5.
[b] Numbers of chondrules used for obtaining the average.
[c] B05 is excluded from the average because B05 composition is higher in SiO_2 and Na_2O than other Al-rich chondrules.
[d] Anorthite-bearing type II chondrules.

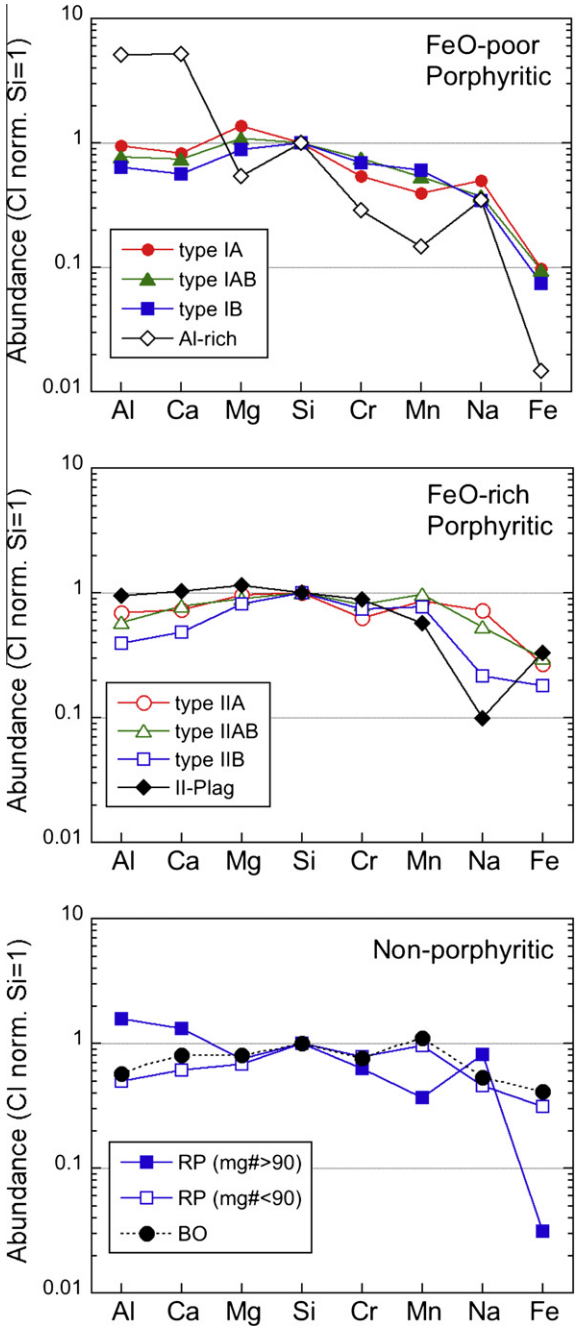

Fig. 2. The abundance of major elements in different types of chondrules in LL3 chondrites. Data in Table 1 are normalized to CI chondrite compositions (Anders and Grevesse, 1989) and Si abundance. The elements are shown in order of increasing volatility, except for Fe, which is placed to the extreme right. (a) Type I (FeO-poor) porphyritic chondrules. (b) Type II (FeO-rich) porphyritic chondrules. (c) Non-porphyritic chondrules.

CH61 contain both forsterite with darker reddish CL and bright blue CL, which are heterogeneously distributed. Other chondrules do not show strong CL signals. Large dusty olivine grains were found in one type IAB chondrule (K10). Another type IA chondrule (K24) also contains minor dusty olivine grains. Type IIAB chondrule B39 contains large phenocryst olivine grains with Mg-rich cores (~Fo_{90}) compared to average olivine compositions (Fo_{74}). However, none of type II chondrules studied contain nearly pure forsteritic (>Fo_{99}) relict olivine.

The anorthite-bearing type II chondrules were recognized in LL3 chondrites in previous Al–Mg chronology studies as a minor group of ferromagnesian chondrules (Kita et al., 2000, 2005; Mostefaoui et al., 2002). Although they contain anorthite, their bulk chemical compositions are not Al-rich ($Al_2O_3 < 10\%$). They also show depleted moderately volatile elemental abundances (i.e., Na and Mn) compared to normal type II chondrules (Fig. 2b). These FeO-rich, anorthite-bearing chondrules may be related to the so-called "clast chondrule" 1805-C1 in Semarkona studied by Hutcheon and Hutchison (1989), who considered the chondrule (C1) to be a fragment of igneous rock from a differentiated asteroid. However, their bulk chemical compositions are generally CI-like (Fig. 2), which is inconsistent with differentiated materials. Furthermore, the Mg contents of anorthite in these chondrules (~0.5% MgO; Kita et al., 2000; Mostefaoui et al., 2002) are much higher than those in anorthite in achondrites. For these reasons, we consider them as one type of FeO-rich chondrule containing anorthite.

3.2. Oxygen isotopes in chondrules: general trend

In the first 2 analytical sessions using 15 μm primary beam spots, we obtained a total of ~160 oxygen isotope analyses from olivine and pyroxene in 36 chondrules. The number of analyses per chondrule varies between 2 and 9. In addition to olivine and pyroxene, several spots of glassy mesostasis in four chondrules in Bishunpur and Krymka (B4, B26, K10, and K27) were analyzed. Since the mesostasis in most chondrules is a fine-grained mixture of glassy mesostasis and clinopyroxene micro-crystallites, an additional 40 analyses were made using a 5-μm beam spot on 6 chondrules in Semarkona (CH4, CH11, CH33, CH36, CH44, and CH52) in order to compare oxygen isotope ratios in phenocrysts, fine-grained clinopyroxene, and glassy mesostasis in each chondrule. All analyses (321 spots, including 209 chondrule analyses and 112 standard analyses) are shown in Table EA7-1 (in the order of analysis sequence) and summarized in Table EA7-2 (in the order of chondrule types).

As shown in Fig. 4a, most data plot on or slightly above the terrestrial mass fractionation (TF) line with a significant range of $\delta^{18}O$ values (0–6‰). Only a few points plot significantly below the TF line, which are obtained from four chondrules (CH44, CH61, B47, and CH26, Fig. 4b). In most chondrules, oxygen isotope ratios in olivine and pyroxene do not show detectable variation within a single chondrule ($2SD \leqslant 1‰$ in both $\delta^{18}O$ and $\delta^{17}O$; see Table EA7-2). For these samples, the average values of phenocryst analyses for each chondrule are calculated and shown in Table 2 and Fig. 4c. The uncertainties of the average values in individual chondrules were estimated from twice the standard error of the mean (2SE) of multiple data (n), unless it is smaller than the weighted average of data ($2SE = 2SD$ of bracketing standard analyses divided by

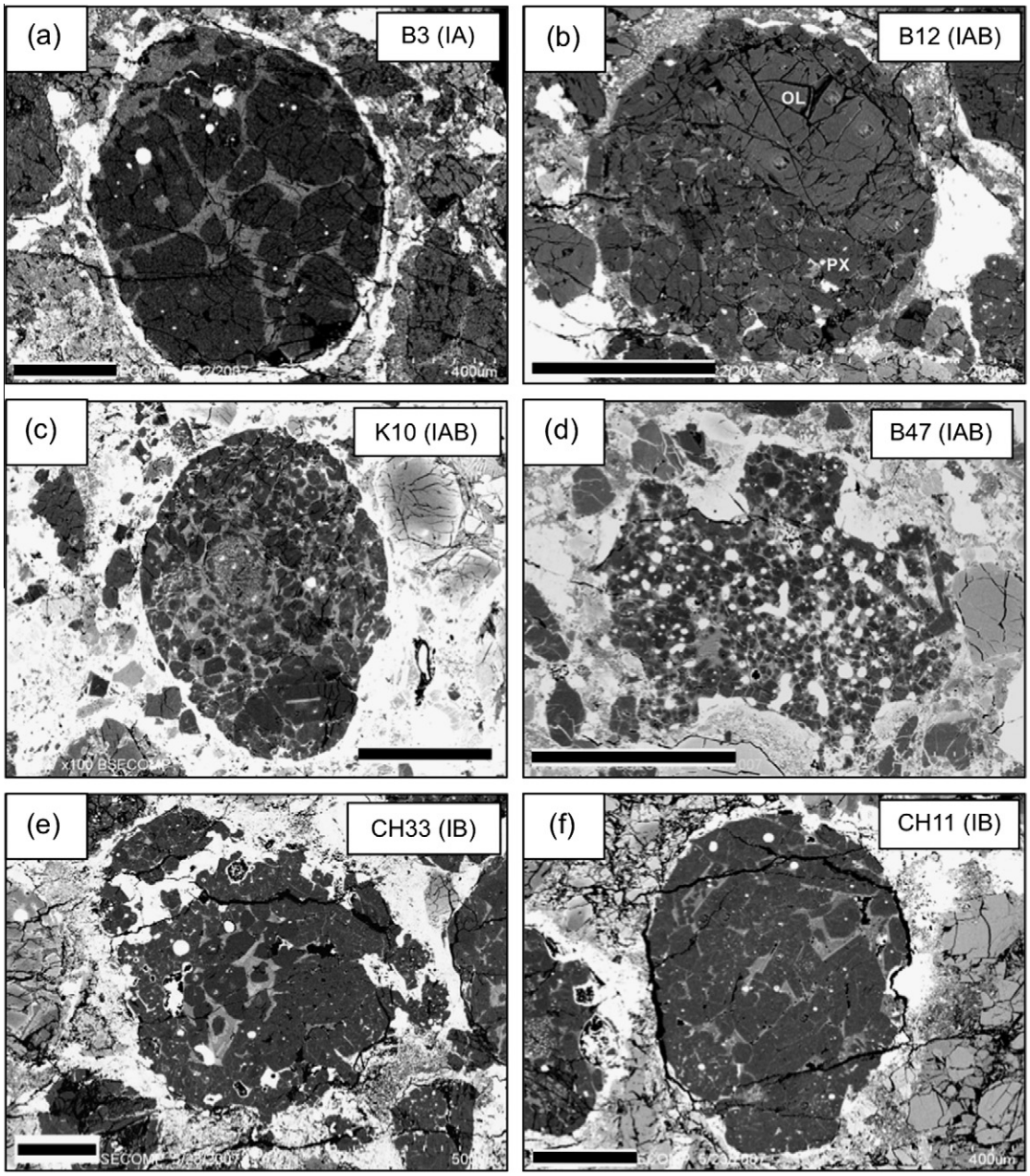

Fig. 3. Representative types of chondrules in LL3.0–3.1 studied for oxygen isotope ratios by SIMS. BSE images with scale bars of 200 μm. (a) Type IA chondrule B3 consists of forsteritic olivine and Ca, Al-rich glass. (b) In type IAB chondrule B12, a large olivine phenocryst occupies half of the chondrule, with the remainder mostly pyroxene. (c) Type IAB chondrule K10 consists of olivine, low Ca pyroxene and glass. A dusty olivine grain with numerous reduced metal grains is located at the center. (d) Type IAB chondrule B47 shows an irregular outer shape and consists of small ($\leqslant\sim$10 μm) olivine phenocrysts. Pyroxene (slightly lighter gray compared to olivine) is concentrated at the edge of the chondrule. This chondrule also contains abundant metal particles and has a fine-grained rim. These characteristics are not typical of UOC chondrules, but are similar to chondrules in carbonaceous chondrites. (e) Type IB chondrule CH33 contains olivine phenocrysts at the center and pyroxene phenocrysts near the edge. (f) Type IB chondrule B11 is mostly enstatite rimmed with a thin (<10 μm) high Ca pyroxene. (g) Type IIA chondrule CH52 consists of FeO-rich olivine (Fo77) phenocrysts and high Ca pyroxene micro-crystallites included in SiO_2-rich glass. (h) Type IIAB chondrule CH26 consists of FeO-rich olivine and pyroxene phenocrysts. The white arrow indicates the olivine grain that shows a large ^{16}O-enrichment. (i) radial pyroxene (RP) chondrule B11 consists of fine-grained (<10 μm) low Ca pyroxene and mesostasis. (j) Anorthite-bearing type II (II-PL) chondrule CH23 consists of olivine, pyroxene and plagioclase in non-porphyritic texture.

the square root of n). Furthermore, additional 0.3‰ and 0.15‰ uncertainties in instrumental bias corrections for $\delta^{18}O$ and $\delta^{17}O$, respectively, are propagated to the final average values as described earlier. The calculation of uncertainties in the average values is shown in Table EA7-2.

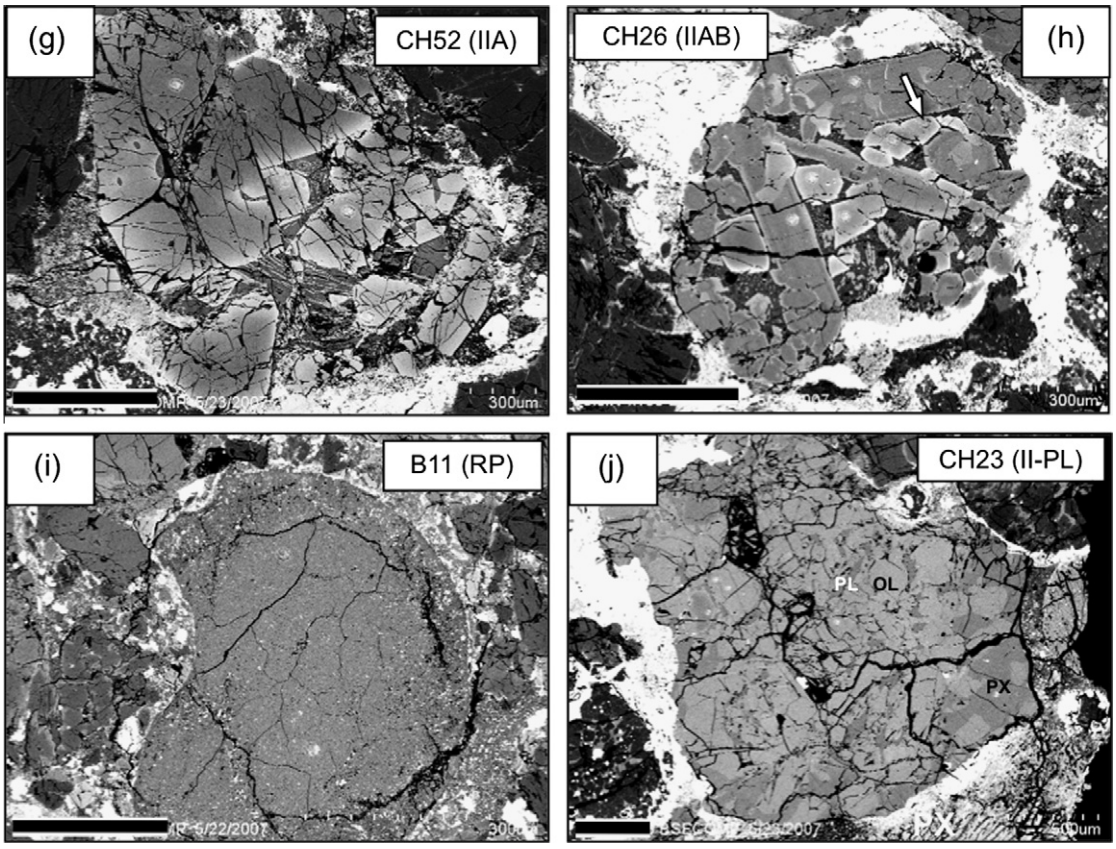

Fig. 3 (*continued*)

The average oxygen isotope ratios of individual chondrules show systematic variations among different chondrule types, although the variation among types may overlap (Fig. 4c). Type I chondrule data show a wide range of $\delta^{18}O$ values from +1‰ to +6‰, which generally increase in the order of IA, IAB and IB, from olivine-rich to pyroxene-rich chondrules. In particular, data from type IA chondrules plot systematically on the left side of the Y&R line; this range of values is not observed from bulk chondrule analyses by Clayton et al. (1991). The Al-rich chondrule CH5 also shows a similar light isotope enrichment (i.e., low $\delta^{18}O$), which confirms our previous result using an IMS-1270 (Nagahara et al., 2008). Type IA chondrules are generally smaller than 1 mm (Jones and Scott, 1989) and might not have been sampled in previous bulk analyses that required more than a few mg of material (Clayton et al., 1991), equivalent to 1 mm in diameter. Among the type IB, CH33 plots on the left side of the Y&R line, similar to type IA chondrules. Unlike other type IB chondrules, CH33 shows a layered structure with olivine phenocrysts located at the center of the chondrule, and surrounded by glassy mesostasis and pyroxene phenocrysts (Fig. 3e).

In contrast to the wide variation among type I chondrules, type II chondrules (IIA, IIAB, IIB, RP and II-PL) cluster at $\delta^{18}O \sim 4.5‰$ and $\delta^{17}O \sim 2.7‰$ ($\Delta^{17}O \sim 0.5‰$), and do not vary more than 1‰ in both $\delta^{17}O$ and $\delta^{18}O$ (Fig. 4c). The average values for types IIA, IIAB, IIB, and RP are $\delta^{18}O = 4.51 \pm 0.44‰$, $\delta^{17}O = 2.89 \pm 0.60‰$, and $\Delta^{17}O = 0.54 \pm 0.60‰$ (2SD, $n = 14$). There is no obvious difference among type II chondrules with respect to olivine and pyroxene modal percentages (e.g., types A, AB, and B). However, anorthite-bearing type II chondrules (CH23, B29, B38, and K21; labeled as "II-Plag" in Fig. 4c) all plot near the TF line with an average, $\Delta^{17}O = 0.14 \pm 0.30$ ($n = 4$, 2SD). The bulk chemical compositions of these anorthite-bearing chondrules are depleted in volatile elements (Na and Mn) and slightly enriched in refractory elements (Ca and Al) compared to other type II chondrules (Fig. 2b). Analogous to Al-rich chondrules with ^{16}O-enrichments (Russell et al., 2000), the anorthite-bearing type II chondrules may have more contribution from refractory elements and ^{16}O-rich precursors than normal type II chondrules.

As shown in Fig. 5, the average $\Delta^{17}O$ values of olivine and pyroxene in individual chondrules are distributed widely from $-8.8 \pm 0.3‰$ in B47 (IAB) to $1.6 \pm 0.2‰$ in K25 (IAB), though the majority of chondrules are within a restricted range between 0‰ and 1‰. The average $\Delta^{17}O$ of all chondrules (Fig. 5), excluding those with large ^{16}O-enrichments, is $0.51 \pm 0.87‰$ (2SD), which is systematically lower than the average of bulk chondrules in LL3, as well as the average bulk LL3 chondrites ($0.99 \pm 0.82‰$ and $1.10 \pm 0.20‰$, 2SD, respectively; Clayton et al., 1991). As shown in Fig. 5, type I chondrules show a relatively larger scatter in $\Delta^{17}O$ than type II chondrules. Among type I chondrules, $\Delta^{17}O$ in four type IB chondrules are identical

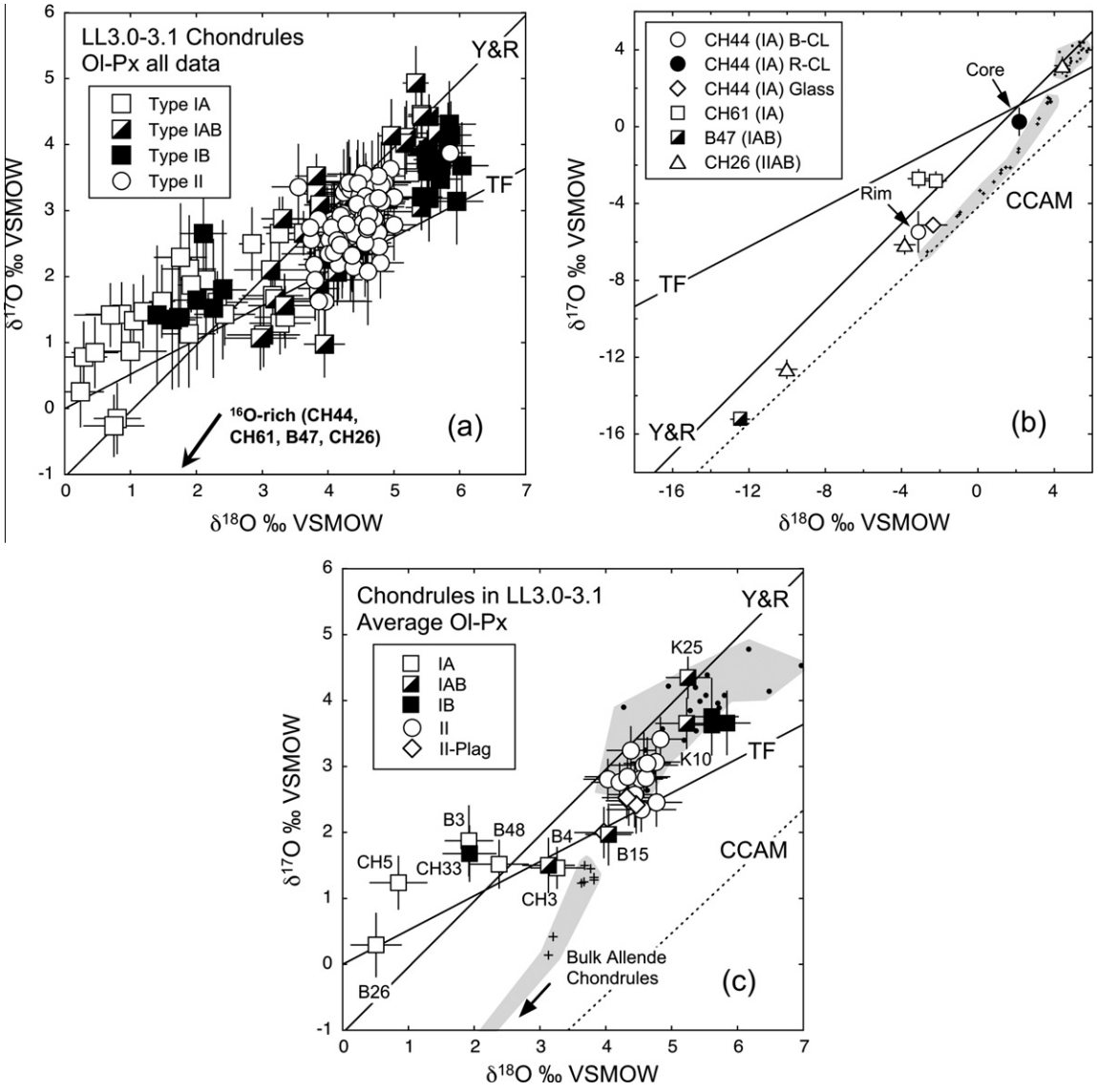

Fig. 4. Oxygen three isotope ratios in chondrules from LL3.0–3.1 chondrites. "TF" and "Y&R" represent the terrestrial mass fractionation line and the Y&R line ($\delta^{17}O = \delta^{18}O - 1.04$; from Young and Russell, 1998), respectively. (a) Individual spot data (~15 μm spots) from olivine and pyroxene excluding four chondrules that plot below the TF line. Data are from Table EA7-2. Type I chondrule data generally plot along a slope = 0.5 line above the TF line with $\delta^{18}O$ increasing from type IA, IAB and IB, while type II chondrule data plot within a narrow range. (b) ^{16}O-rich chondrule data from CH44, CH61 (type IA), B47 (IAB) and CH26 (IIAB). Individual spot analyses are shown for CH61 and olivine grain 3 in CH26. The average values of multiple spot analyses are shown for B47, CH26 (excluding grain 3) and red CL olivine, blue CL olivine, and glass in CH44 (see Tables 2 and 3). Dashed line is the CCAM line (e.g., Clayton, 1993; Clayton et al., 1977). Small dots and crosses are bulk oxygen isotope analyses of chondrules from CV3 and UOCs (shown in Fig. 1), which are outlined by the grey area. (c) The average olivine and pyroxene data of the individual chondrules that show internally homogeneous oxygen isotope ratios near and above TF line. The average values are from Table 2. Anorthite-bearing type II chondrules (labeled as "II-Plag") are shown as open diamonds and plot at the lower ends of the variation among type II chondrules (open circles). An Al-rich chondrule CH5 is shown as IA chondrule symbol. Small dots and crosses are the same as in (b).

within the analytical uncertainties with an average $\Delta^{17}O = 0.73 \pm 0.18‰$ (2SD), in contrast to the larger variation among olivine-rich types IA and IAB chondrules.

3.3. ^{16}O-enriched chondrules and relict olivine grains

Four chondrules (CH44, CH61, B47, and CH26; Tables 2 and 3) partly or uniformly show large ^{16}O excesses and plot below the TF line (Fig. 4b) in a similar region to Al-rich chondrules (Russell et al., 2000). The four chondrules are not Al-rich and belong to three different types (IA, IAB and IIAB), indicating that a ^{16}O-rich solid could be common precursor of UOC chondrules. In Fig. 4b, the ^{16}O-rich data from these chondrules deviate from the Y&R line towards the CCAM line, except for CH61. This is contrary to the trend for Al-rich chondrules reported

Table 2
The average oxygen isotope ratios of olivine and pyroxene in individual chondrules[a] from LL3.0–3.1 chondrites, Semarkona, Bishunpur and Krymka, measured by IMS-1280 SIMS.

Sample name (type)	n[b]	$\delta^{18}O$	Error	$\delta^{17}O$	Error	$\Delta^{17}O$	Error	mg#[c]
CH5 (Al-rich)	3	0.85	0.43	1.24	0.40	0.79	0.45	99.6
B3 (IA)	4	1.92	0.36	1.87	0.53	0.87	0.53	99.0
B4 (IA)	3	3.26	0.40	1.46	0.31	−0.23	0.30	97.0
B26 (IA)	5	0.51	0.38	0.28	0.48	0.03	0.55	97.5
B48 (IA)	2	2.38	0.32	1.52	0.33	0.28	0.29	95.6
K24 (IA)	6	2.3	1.1	2.1	0.6	0.87	0.20	95
CH3 (IAB)	5	3.13	0.39	1.50	0.41	−0.13	0.35	96.3
B12 (IAB) olivine	3	3.65	0.46	3.22	0.40	1.32	0.23	93
Pyroxene-core	1	4.91	0.31	3.17	0.33	0.62	0.30	96
Pyroxene-rim	2	5.60	0.37	4.30	0.30	1.39	0.32	95.5
B15 (IAB)	6	4.04	0.34	1.97	0.46	−0.13	0.40	94
B47 (IAB)	2	−12.46	0.49	−15.22	0.36	−8.78	0.29	96.6
K10 (IAB)	6	5.23	0.47	3.65	0.38	0.94	0.31	97
Dusty olivine	3	3.89	0.43	2.78	0.34	0.76	0.36	
K25 (IAB)	6	5.25	0.33	4.35	0.31	1.62	0.24	96
CH11 (IB)	5	5.84	0.35	3.66	0.48	0.63	0.44	98
CH33 (IB)	7	1.93	0.40	1.68	0.42	0.67	0.40	99
B10 (IB)	4	5.61	0.34	3.63	0.29	0.71	0.23	96
Olivine phenocryst	1	4.59	0.30	2.76	0.50	0.38	0.47	96
B13 (IB)	3	5.61	0.40	3.76	0.58	0.84	0.45	98
CH52 (IIA)	5	4.58	0.51	3.02	0.49	0.64	0.39	77
B43 (IIA)	4	4.03	0.36	2.81	0.30	0.71	0.26	90
K15 (IIA)	3	4.53	0.33	2.81	0.24	0.45	0.18	81
CH4 (IIAB) olivine	5	4.83	0.35	3.41	0.33	0.90	0.29	81
Pyroxene	4	3.98	0.46	3.22	0.36	1.15	0.32	
CH36 (IIAB)	6	4.21	0.42	2.76	0.29	0.57	0.23	76
B21 (IIAB)	4	4.54	0.52	2.35	0.33	−0.01	0.26	71
B39 (IIAB)	4	4.76	0.36	3.07	0.30	0.60	0.26	74
K27 (IIAB)	4	4.61	0.32	2.83	0.22	0.43	0.17	75
CH60 (IIB)	4	4.38	0.36	3.24	0.36	0.96	0.32	86
B6 (IIB)	5	4.63	0.35	3.05	0.39	0.64	0.30	87
B37 (IIB)	2	4.44	0.39	2.57	0.49	0.27	0.38	91
B11 (RP)	2	4.33	0.64	2.85	0.28	0.59	0.21	82
K19 (RP)	1	4.77	0.38	2.46	0.36	−0.02	0.23	85
CH23 (II-Plag)	5	3.97	0.44	2.00	0.38	−0.06	0.30	83
B29 "BI-C4" (II-Plag)	4	4.35	0.34	2.48	0.37	0.22	0.32	83
B38 "B1-C18" (II-Plag)	4	4.46	0.39	2.42	0.43	0.10	0.34	77
K21 (II-Plag)	4	4.32	0.37	2.53	0.31	0.28	0.25	81

[a] The average values and the associated uncertainties (in 95% confidence level) of individual chondrules were calculated in Table EA7-2.
[b] The number of multiple spot analyses.
[c] Molar [MgO]/[MgO + FeO]% of olivine and pyroxene phenocrysts from Tables EA4 to EA5.

by Russell et al. (2000), which plot slightly above the Y&R line, like CH61.

The CL image of CH44 (IA, Fig. 6) reveals reversely zoned forsterite phenocrysts, $Fo_{99.3}$ cores with red CL and $Fo_{99.7}$ rim with blue CL that are enriched in Al and Ca (Table EA6). The resorption texture indicates that red-CL olivine cores are relict and blue-CL rims are overgrowths from an Al- and Ca-rich melt. In this chondrule, olivine overgrowths and glass have ^{16}O-rich compositions ($\Delta^{17}O = -4.3‰$ and $-3.9‰$, respectively), while the relict olivine cores are relatively ^{16}O-depleted ($\Delta^{17}O = -0.8‰$) and lie closed to the TF line.

Chondrule CH61 consists of abundant forsteritic olivine with complex CL zoning profiles. We obtained only two data points due to the small olivine grain sizes in this chondrule. Although data from CH61 are displaced significantly below the TF line compared to other type IA chondrules, the data also plot above the Y&R line like other type IA chondrules.

Data from B47 (type IAB) show the most ^{16}O-rich compositions and are close to the CCAM line ($\delta^{18}O \sim -12.5‰$ and $\delta^{17}O = -15.2‰$). The value of $\Delta^{17}O = -8.8 \pm 0.3‰$ observed from this chondrule is even lower than those of Al-rich chondrules in UOCs ($\Delta^{17}O \geqslant -6‰$; Russell et al., 2000). It is interesting to note that the texture of this chondrule, shown in Fig. 3d, somewhat resembles those in CO chondrites, such as small olivine phenocrysts, enrichment of pyroxene at the periphery of the chondrule, abundant small metal grains, and relatively thick fine-grained rims (e.g., Kurahashi et al., 2008).

CH26 is the only type II chondrule that shows a significant degree of ^{16}O-enrichment (Fig. 4b). This ^{16}O-enrichment is only observed in one olivine grain (Fig. 3h), while the rest of the data for this chondrule plot above the TF line

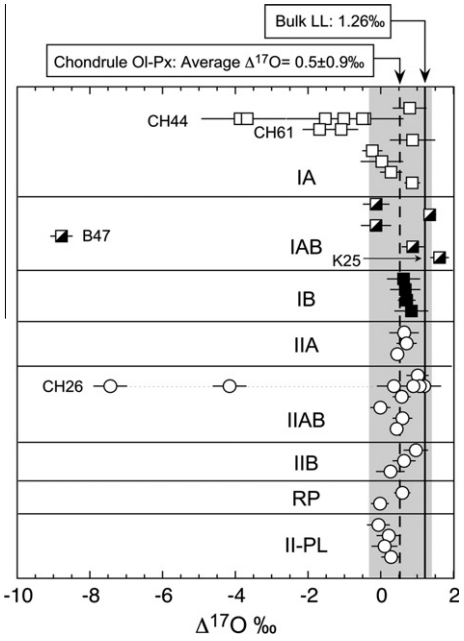

Fig. 5. The average $\Delta^{17}O$ values of olivine and pyroxene from individual chondrules in LL3.0–3.1 chondrites. The average values of olivines and pyroxenes (15 μm spot) from individual chondrules (Table 2) are shown, while individual spot analyses are shown for three chondrules (CH44, CH61, and CH26) containing relict olivine grains. The average of all the chondrules (excluding CH44, CH61, B47, and CH26) is $0.5 \pm 0.9‰$ (2SD), is shown by a dashed line. The solid line is the average LL4–LL6 chondrite bulk $\Delta^{17}O$ value (Clayton et al., 1991).

within the range of other type II chondrules (Fig. 4b). There is no obvious petrographic indication of the ^{16}O-rich grain being relict, such as higher Fo content. Therefore, the occurrence of relict ^{16}O-rich olivine in this chondrule is quite different from that in type II chondrules in CO3 and Acfer 094 that show relict Fo grains (Kunihiro et al., 2004, 2005).

3.4. Heterogeneity within individual ^{16}O-poor chondrules

Five chondrules (K10, K24, B12, B10, and CH4) analyzed with 15 μm spots show resolvable internal heterogeneity in $\delta^{18}O$ that is more than 1‰ beyond the analytical precision (0.2–0.7‰). Individual spot analyses and the average of analyses with different petrographic domains are shown in Table EA-7 and Table 2, respectively. Two chondrules containing dusty olivine grains in Krymka (K10 and K24) show more than 1‰ variation in $\delta^{18}O$ parallel to the TF line (Fig. 7a). Chondrule K10 (IAB) contains a large dusty olivine grain at the center (Fig. 3c), which has $\delta^{18}O$ values that are lower than the host olivine and pyroxene by 1–2‰. Another chondrule (K24, type IA) contains dusty olivine grains and shows variation in $\delta^{18}O$ of ~3‰, though no data are from the dusty olivine grains because they were too small and difficult to analyze.

The chondrule, B12 (IAB), contains a large olivine phenocryst that occupies nearly one-half of the chondrule, while the rest of the chondrule consists of pyroxene (Fig. 3b). Three analyses of the olivine grain are homogeneous, and their average is lower in $\delta^{18}O$ than those of the pyroxene grains (Fig. 7b). Two analyses of pyroxene at the periphery of the chondrule ("Rim" in Fig. 7b) are higher in both $\delta^{18}O$ and $\delta^{17}O$ compared to the analyses of pyroxenes located at the center of the chondrule ("Center" in Fig. 7b). The average olivine data and "Rim" pyroxene data plot parallel to the TF line with relatively high $\Delta^{17}O$ of 1.3–1.4‰. The chondrule, B10 (IB), contains one olivine phenocryst (~150 μm) which shows $\delta^{18}O$ and $\delta^{17}O$ that are lower than pyroxene by 1‰. The analysis of an olivine chadacryst in the same chondrule (~30 μm) shows oxygen isotope ratios that are indistinguishable from that of the pyroxene (see Table EA7-2), indicating that the olivine chadacryst and pyroxene grew together, while the larger olivine grain is probably relict.

In the chondrule, CH4 (IIAB), the oxygen isotope ratios at the center of large olivine phenocrysts are homogeneous (average value with 15 μm spot; $\delta^{18}O = 4.83 \pm 0.16‰$, $n = 5$, 2SD, Table EA7-2), while the pyroxene phenocrysts are lower in $\delta^{18}O$ (3.9–4.4‰) than the olivine and both plot along a mass dependent fractionation line (Fig. 7b).

3.5. Mesostasis of selected chondrules

We analyzed glass from 9 chondrules (B4, B26, K10, CH11, CH33, CH52, CH4, CH36, and K27) to test whether the glass exchanged with "^{16}O-poor" nebular gas during the melting of the chondrules. In four chondrules (CH11, CH33, CH4, and CH36), co-existing high Ca-pyroxenes ("Cpx") in the same chondrules were also analyzed for comparison. As shown in Fig. 8, Cpx in these chondrules occurs as overgrowths at the rim of low-Ca pyroxene phenocrysts, and as small crystals in the mesostasis. These analyses are summarized in Table 4 and are plotted together with the averages of the olivine and pyroxene data in Fig. 9. The oxygen isotope data in the chondrule glasses are widely distributed, in contrast to the limited range of variations observed from the olivine and pyroxene. The glass data in chondrules CH33 and CH4 show similar $\delta^{18}O$ and $\delta^{17}O$ values to the olivine and low-Ca pyroxene in the same chondrules. In other chondrules, such as CH52, CH36, and K27, oxygen isotope ratios in glass are significantly higher in both in $\delta^{18}O$ and $\delta^{17}O$ than olivine and low-Ca pyroxene. The highest values are $\delta^{18}O = 17‰$, $\delta^{17}O = 14‰$ and $\Delta^{17}O = 5‰$ found in CH36.

Because of the small grain size, clean Cpx analyses were made only in CH4 and CH33, which are in good agreement with the analyses of olivine and pyroxene in the same chondrules. Some Cpx analysis spots in CH36 overlapped with glass (labeled as "G + Cpx"). The $\delta^{18}O$ and $\delta^{17}O$ values of these mixed analyses are generally proportional to the fraction of glass observed in the analytical spot, indicating that the Cpx grains in the mixed analysis spots do not have extremely high $\delta^{18}O$ and $\delta^{17}O$ values.

4. DISCUSSION

4.1. Origin of heavy oxygen isotopes in chondrule glass

4.1.1. Effect of aqueous alteration

In this work, we observed large variation in oxygen isotope ratios of glass among chondrules, which are enriched

Table 3
Oxygen isotope ratios of individual spots in chondrites[a] with ^{16}O-enriched olivine grains, measured by IMS-1280 SIMS.

Sample name (type)	$\delta^{18}O$	Error	$\delta^{17}O$	Error	$\Delta^{17}O$	Error	mg#[c]
CH44 (IA)							
#2-olivine (red CL)	1.9	0.4	−0.5	1.0	−1.5	1.0	99.2
#3-olivine (red CL)	2.3	0.4	0.7	1.0	−0.4	1.0	99.3
#4-olivine (red CL)	2.3	0.4	0.7	1.0	−0.5	1.0	
#6-olivine (red CL)	2.2	0.4	0.1	1.0	−1.0	1.0	
#9-olivine (red CL)[b]	3.0	0.9	1.0	0.5	−0.6	0.8	
#7-olivine (red/blue CL)[b]	1.5	0.9	−0.9	0.5	−1.7	0.8	
#1-olivine (blue CL)	−3.1	0.4	−5.5	1.0	−3.9	1.0	99.7
#11-olivine (blue CL)[b]	−2.7	0.9	−5.9	0.5	−4.5	0.8	
#10-glass[b]	−2.4	0.9	−5.3	0.5	−4.0	0.8	
#8-glass[b]	−2.3	0.9	−5.0	0.5	−3.8	0.8	
Red CL olivine average ($n = 4$)	2.2	0.4	0.3	0.7	−0.9	0.5	
Blue CL olivine average ($n = 1$)	−3.1	0.5	−5.8	1.1	−3.9	1.0	
Glass average ($n = 2$)	−2.4	0.7	−5.1	0.4	−3.9	0.5	
CH61 (IA)							
Olivine-1	−2.2	0.5	−2.8	0.5	−1.7	0.4	
Olivine-2	−3.1	0.5	−2.7	0.5	−1.1	0.4	
CH26, IIAB							
Olivine-1	4.3	0.5	3.3	0.5	1.1	0.4	75.7
Olivine-2	4.5	0.5	3.6	0.5	1.2	0.4	78.8
Olivine-3-1	−10.0	0.5	−12.6	0.5	−7.4	0.4	77.1
Olivine-3-2	−3.8	0.5	−6.1	0.5	−4.2	0.4	
Pyroxene-1	4.5	0.5	3.2	0.5	0.9	0.4	
Pyroxene-2	4.3	0.5	2.6	0.5	0.4	0.4	
Average (excluding olivine-3)	4.43	0.40	3.18	0.43	0.88	0.37	

[a] Error quoted to individual data are from 2SD of bracketing standard analyses, while those for the average values are weighted errors of multiple data.
[b] The spots sized are 5 μm (S3), otherwise 15 μm (S1).
[c] Molar [MgO]/[MgO + FeO]% of olivine phenocrysts from Table EA5.

in both $\delta^{18}O$ and $\Delta^{17}O$ compared to minerals in the same chondrules. If Cpx in chondrule mesostasis and at the rim of phenocrysts crystallized from chondrule melt and they were in oxygen isotope equilibrium with the melt at high temperature, Cpx and glass oxygen isotope data should show identical $\Delta^{17}O$ and small a difference in $\delta^{18}O$ less than 1‰ (e.g., Zhao and Zheng, 2003). Although only a few analyses were successful for Cpx in this study due to small grain sizes, our glass data consistently show much higher $\Delta^{17}O$ and $\delta^{18}O$ than Cpx, while Cpx data are in good agreement with those of phenocrysts in the same chondrules. Two possible explanations of these observations are: (1) oxygen isotope ratios in the chondrule melt dramatically changed after Cpx crystallization due to isotope exchange with ambient gas, and (2) the oxygen isotope ratios in glass were altered much later during fluid–rock interaction on the chondrite parents bodies. Crystallization temperature of Cpx may not be significantly different from the glass transition temperature of silicate melt. The first explanation is unlikely because it requires sudden changes in oxygen isotope ratios in the ambient gas right after Cpx crystallization.

In Fig. 10, glass data are summarized in an oxygen three-isotope diagram, and show a linear trend with a slope of ~0.8. The oxygen isotope ratios of feldspar/glass concentrates (low density separates) from chondrules and bulk UOCs (Bridges et al., 1999) plot within the range of SIMS analyses of chondrule glasses. The highest $\delta^{18}O$ and $\delta^{17}O$ values of glass in CH36 plot along mass fractionation line defined by matrix magnetite in Semarkona (Choi et al., 1998), which is considered to be the product of aqueous alteration in the parent body (Krot et al., 1997). Therefore, glass might have exchanged oxygen isotopes with an aqueous fluid having high $\Delta^{17}O$ values (~5‰) in the LL3 parent body. As discussed by Choi et al. (1998), oxygen isotopic equilibrium may not have been achieved between magnetite in the matrix and glass in chondrules. However, here we assessed the oxygen isotope fractionation between magnetite and chondrule glass to test whether they equilibrated at low temperature (⩽260 °C suggested to be the peak metamorphic temperature experienced by Semarkona; Alexander et al., 1989). Here we assume the oxygen isotope fractionation factor between CH36 glass and magnetite to be similar to that between albite and magnetite, because the major element composition (especially SiO_2 wt%) of CH36 glass is similar to albite. We assume the $\delta^{18}O$ value of matrix magnetite to be 0.4 ± 1.1‰ from the average of 10 Semarkona matrix magnetite analyses by Choi et al. (1998). The oxygen isotope fractionation, defined as $\Delta^{18}O(\text{glass-matrix}) = \delta^{18}O(\text{CH36 glass}) - \delta^{18}O(\text{matrix magnetite})$, is ~17‰, which is similar to that of albite–magnetite; $\Delta^{18}O(\text{albite–magnetite}) = 16.7$‰ at $T = 250$ °C using the equation in Clayton and Kieffer (1991). Therefore, it is likely that glass in chondrule CH36 experienced

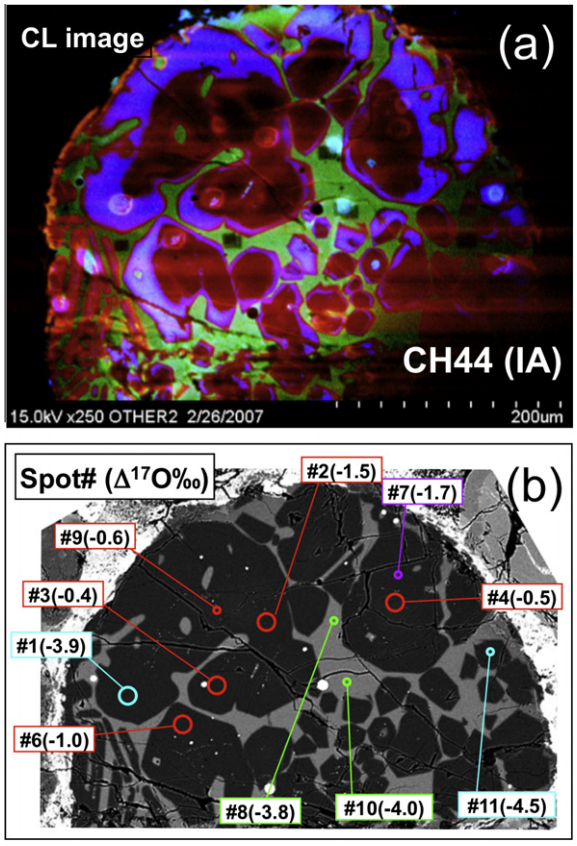

Fig. 6. Type IA chondrule CH44, showing ^{16}O-poor relict forsterite overgrown by ^{16}O-rich olivine rim in an Al–Ca-rich glass. (a) Color CL image of CH44, by combining three images taken with red, green, and blue filters (brightness of individual color signals was not calibrated). Blue CL olivine grains have higher Fo contents ($\sim Fo_{99.7}$) than red CL olivine grains ($\sim Fo_{99.3}$) and are enriched in refractory minor elements (CaO and Al_2O_3). (b) BSE image of CH44 with the positions of SIMS spots and Δ^{17}O values. The diameters of circles indicate the analysis spot sizes of 15 and 5 μm. Red, blue and green circles represent the analysis positions from red CL olivine, blue CL olivine and green CL glass.

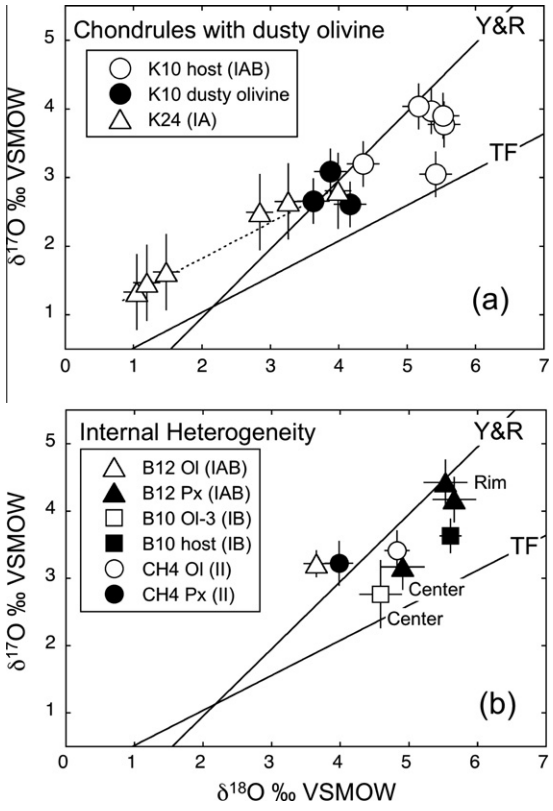

Fig. 7. Oxygen isotope ratios of chondrules showing resolvable internal heterogeneity. "TF" and "Y&R" represent terrestrial mass fractionation and Young and Russell lines, respectively. (a) Chondrules K10 (IAB) and K24 (IA) contain dusty olivine grains. (b) Chondrules B12, B10, and CH4. The average values are shown for B12 olivine ($n = 3$, from a single large olivine phenocryst), B10 host ($n = 4$, 1 olivine and 3 pyroxenes), CH4 olivine ($n = 5$, 15 μm spots only) and CH4 pyroxene ($n = 4$, 15 μm spots only). Other data are from a single spot analyses.

almost complete oxygen isotope exchange with an aqueous fluid in the parent body. Experimental data are not available for oxygen isotope diffusion in glass at temperatures below 500 °C. Extrapolation of the existing diffusion data (Behrens et al., 2004, 2007; see EA8) indicates that oxygen isotope diffusion in glass with water contents of 0.1 wt% may occur at a 10 μm scale for 1 Ma at $T = 250$ °C. Oxygen isotope exchange between chondrule glass and an aqueous fluid seems to be incomplete in most of the other chondrules, which show oxygen isotope ratios that are intermediate between that in CH36 glass and those of the olivine–pyroxene phenocrysts.

Oxygen isotope exchange between chondrule glass and parent body aqueous fluid may be found in another class of type 3 chondrites with low petrographic subtypes ($\leqslant$3.2). Maruyama et al. (1999) and Maruyama and Yurimoto (2003) suggested mesostasis of chondrules in Allende (CV3) might be altered by the aqueous alteration in the parent body. The Δ^{17}O values of mesostasis in Vigarano (CV3) chondrules analyzed by SIMS systematically show values higher than olivine and pyroxene phenocrysts (Chaussidon et al., 2008), which were interpreted as primary isotope ratios in chondrule glass reflecting the solar nebula gas. However, some data plot on the left side of the CCAM line with $\Delta^{17}O \sim -2‰$, similar to that observed in magnetite in Allende CV3 (Choi et al., 1997), could be the result of isotope exchange with aqueous fluid in the CV parent body.

4.1.2. Contribution to whole-rock oxygen isotope ratios

The average of Δ^{17}O value of chondrules, based on the analyses of olivine and pyroxene obtained in this work ($0.5 \pm 0.9‰$, 2SD, Fig. 5), is systematically lower than the average value of bulk LL chondrites ($\sim$1.26‰, Clayton et al., 1991), or those in the host bulk meteorites of these chondrules (1.1‰, 1.0‰, 1.2‰ for Semarkona, Bishunpur and Krymka, respectively; Clayton et al., 1991). From the analyses of chondrule glass in this work and previous studies of matrix magnetite (Choi et al., 1998), it is evident that the most ^{16}O-poor component in the bulk LL chondrites resides in chondrule glass and matrix minerals. Their oxygen isotope ratios probably reflect exchange with a ^{16}O-poor

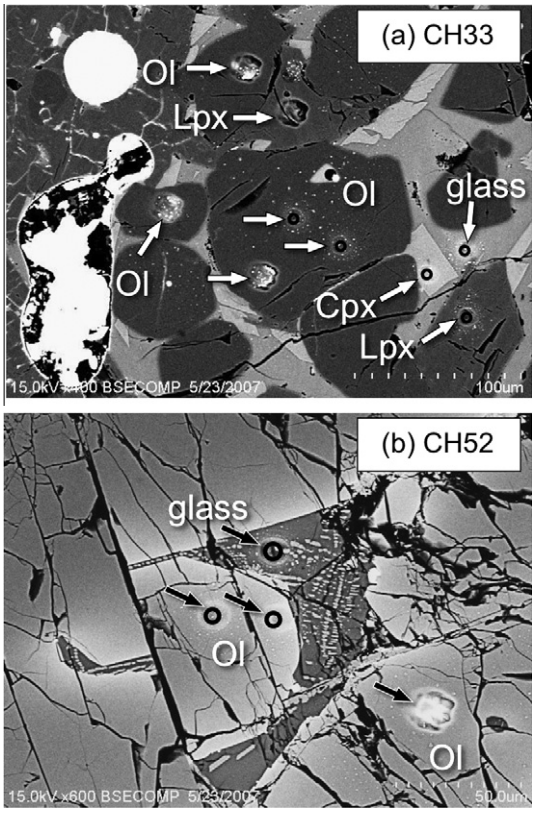

Fig. 8. BSE images of SIMS analysis spots in chondrule mesostasis. (a) CH33 (type IB) and (b) CH52 (type IIA). Arrows indicate SIMS analysis spots. "Ol", olivine; "Cpx", high Ca-pyroxene; "Lpx", low Ca pyroxene. The small 5 μm spots are shown with circles representing the size of SIMS pits. In CH33, some high Ca pyroxene rims are large enough to obtain clean SIMS analyses. In this example, glassy mesostasis is also analyzed adjacent to high Ca pyroxene. In CH52, the glass analysis spot slightly overlaps with pyroxene micro-crystallites.

fluid during aqueous alteration in the LL parent body. The bulk $\delta^{18}O$ values of all three LL3 chondrites are higher than that of the average type 4–6 LL chondrites (5.4–6.1‰ versus 5.0‰; Clayton et al., 1991), which is also consistent with aqueous alteration of components in these LL3 chondrites at lower temperatures.

We suggest that the bulk LL chondrite oxygen isotope ratios were established by the mixing of anhydrous silicates, represented by the average chondrule olivine and pyroxene data, and liquid water (or ice) accreted by the LL parent body. The origin of the water in the ordinary chondrite parent body that resulted in aqueous alteration in type 3 chondrites is not well understood. It could be ice accreted by the parent body, or H_2O released by pyrolysis or oxidation of organic material. If we assume the water content of bulk Semarkona (1.6 wt%, Jarosewich, 1990) as the amount of water that existed in the LL chondrite parent body, the $\Delta^{17}O$ value in the initial water of ~20‰ is estimated to increase the bulk $\Delta^{17}O$ value from 0.5‰ (average chondrules) to 1.1‰ (bulk Semarkona). The highest $\Delta^{17}O$ values ever observed from meteorites are "Cosmic symplectite" (COS), magnetite-sulfide assemblages in a matrix phase of Acfer 094 (ungrouped C chondrite), with $\Delta^{17}O = +80‰$ ($\delta^{18}O = \delta^{17}O \sim 180‰$, Sakamoto et al., 2007). Acfer 094 is the least aqueously altered chondrite (Greshake, 1997), which may preserve unaltered materials accumulated to asteroids. Addition of an extremely ^{16}O-depleted component, similar to those found in COS, would increase the $\Delta^{17}O$ value of fluid significantly.

4.2. Oxygen isotope systematics of chondrules in LL3 chondrites

4.2.1. Primary oxygen isotopes in chondrules estimated from phenocryst data

As discussed above, the primary oxygen isotope ratios in chondrules are most likely represented by olivine and pyroxene phenocrysts, except for rare cases where unmelted (relict) olivine with distinct oxygen isotope ratios are found. Considering that the volume percentage of glass in most chondrules is less than 30%, the oxygen isotope ratios of the average olivine and Low-Ca pyroxene phenocrysts should be close to that of individual bulk chondrules prior to parent body alteration. In contrast, actual bulk chondrule isotope analyses could be easily displaced by more than 1‰, depending on the fraction of glass and the degree of oxygen isotope exchange with aqueous fluid. In the following discussion, the average olivine and pyroxene data from individual chondrules are considered to represent their primary oxygen isotope ratios. In Fig. 11, oxygen isotope ratios obtained from olivine and pyroxene are summarized as $\delta^{18}O$–$\Delta^{17}O$ diagram. Most chondrules plot above the TF line and generally follow a separate mass dependent fractionation line with $\Delta^{17}O$ values between 0‰ and 1‰, below that of bulk LL chondrites ($\Delta^{17}O \sim 1.3‰$). One chondrule (K25, IAB) shows a $\Delta^{17}O$ value as high as $1.6 \pm 0.2‰$ that plot above the bulk LL chondrite (Fig. 5). Type IA chondrule data are fractionated to light isotope enrichments compared to types IAB and B. Type II chondrule data show a narrow range of values. Some chondrules show ^{16}O-enrichment towards the CCAM line, either as a whole or as relict grains. These results significantly extend the range of oxygen isotope ratios in OC chondrules compared to previous bulk analyses (Clayton et al., 1991; Bridges et al., 1998).

The systematic variation in oxygen three-isotope ratios among type I and type II chondrules is also demonstrated in Fig. 12, showing the $\delta^{18}O$ and $\Delta^{17}O$ values of individual chondrules with their mg# of olivine and pyroxene phenocrysts. The figure clearly demonstrates the large mass dependent isotope fractionation (variable $\delta^{18}O$ with constant $\Delta^{17}O$ values) among type I chondrules, especially those with the highest mg#. A large mass dependent isotope fractionation occurred under the conditions that formed magnesian chondrules, possibly under reducing conditions.

4.2.2. Correlation between $\delta^{18}O$ and Mg/Si ratio in type I chondrules

In this study, we found a large mass dependent fractionation in oxygen isotopes among type I chondrules, especially light isotope enrichment in IA. If oxygen isotope fractionation among type I chondrules is caused by

Table 4
Oxygen isotope ratios of high Ca pyroxene (Cpx) and mesostasis (G) compared to olivine (Ol) and low Ca pyroxene (Lpx) in selected chondrules, measured by IMS-1280 SIMS.

Chondrule[a] (type)	Phase	Glass SiO_2%	$\delta^{18}O$	Error	$\delta^{17}O$	Error	$\Delta^{17}O$	Error
B4 (IA)	G	48.5	7.4	0.5	5.4	0.5	1.5	0.4
	G	49.5	5.3	0.5	3.5	0.5	0.7	0.4
	Ol[b]		3.3	0.4	1.5	0.3	−0.2	0.3
B26 (IA)	G	51.9	8.7	0.5	6.6	0.5	2.0	0.4
	G	54.0	3.0	0.5	2.0	0.5	0.4	0.4
	Ol[b]		0.5	0.4	0.3	0.5	0.0	0.6
K10 (IAB)	G	59.7	6.3	0.2	4.7	0.3	1.4	0.2
	Ol[b]		5.2	0.5	3.7	0.4	0.9	0.3
CH11 (IB)	Cpx + G(~30%)		4.8	1.0	2.8	0.8	0.3	0.9
	G	55.2	9.8	1.0	6.7	0.8	1.6	0.9
	G	58.7	7.1	1.0	4.6	0.8	0.9	0.9
	G	57.5	7.9	1.0	5.3	0.8	1.2	0.9
	Ol–LPx[b]		5.8	0.4	3.7	0.5	0.6	0.4
CH33 (IB)	Cpx		2.0	0.8	1.3	0.5	0.3	0.6
	G	56.7	4.6	0.8	2.6	0.5	0.3	0.6
	G	56.5	3.7	0.8	2.4	0.5	0.4	0.6
	Ol–Lpx[b]		1.9	0.4	1.7	0.4	0.7	0.4
CH52 (IIA)	G	70.0	14.5	0.8	10.4	1.0	2.8	1.0
	G (+ Cpx incl.)	69.5	13.6	0.8	9.3	1.0	2.2	1.0
	Ol[b]		4.6	0.5	3.0	0.5	0.6	0.4
CH4 (IIAB)	Cpx		3.3	1.0	3.1	0.8	1.4	0.9
	G[c] ($n = 3$)	67–75	6.1	0.8	4.8	0.5	1.6	0.6
	Ol[b]		4.8	0.4	3.4	0.3	0.9	0.3
	Lpx[b]		4.0	0.5	3.2	0.4	1.2	0.3
CH36 (IIAB)	G + Cpx (<50%)	68.1	12.5	0.8	9.4	1.0	2.9	1.0
	Cpx(50%) + G(50%)		10.3	0.8	7.2	1.0	1.8	1.0
	Cpx(50%) + G(50%)		9.0	0.8	7.1	1.0	2.4	1.0
	G[c] ($n = 2$)	67–71	17.3	0.6	13.8	0.7	4.8	0.7
	Ol–Lpx[b]		4.2	0.4	2.8	0.3	0.6	0.2
K27 (IIAB)	G	65.4	12.5	0.2	9.9	0.3	3.3	0.2
	Ol–Lpx[b]		4.6	0.3	2.8	0.2	0.4	0.2

[a] rror quoted to individual data are from 2SD of bracketing standard analyses, while those for the average values are weighted errors of multiple data.
[b] Olivine and low Ca pyroxene data from Table 2.
[c] The average value of multiple spots (see Table EA 7-2).

the Rayleigh distillation process, such as evaporation of silicate melt in the solar nebula, chondrules with heavy and light isotope enrichments may correspond to evaporation residues and re-condensates from evaporated species, respectively. According to $\delta^{18}O$ values, type IA (lower $\delta^{18}O$) and IB (higher $\delta^{18}O$) chondrules may correspond to condensates and evaporated residues, respectively. However, Jones (1994) reported that type IA chondrules are generally enriched in refractory elements and depleted in volatiles (such as Mn and Na), while type IB chondrules are slightly enriched in moderately volatile elements. The major element data shown in Fig. 2a are consistent with this previous study. Therefore, a Rayleigh distillation process can not explain both the isotopic and chemical difference between types IA and IB chondrules. Furthermore, the $\delta^{18}O$ values in type I chondrules show a negative correlation with the bulk Mg/Si ratios (Table EA5), as shown in Fig. 13a. Because Si is less refractory than Mg (e.g., Wang et al., 2001), a positive correlation would be seen if the oxygen isotopes were fractionated by a Rayleigh distillation process in contrast to the actual observation.

In addition to type IA chondrules, an Al-rich chondrule (CH5) also shows low $\delta^{18}O$ values, though CH5 does not have a high Mg/Si ratio. In this chondrule, Nagahara et al. (2008) observed an inward diffusion of Si and Na from the periphery of the chondrule, which they interpret as evidence for recondensation of Si and alkali elements in the glass. According to the model of Nagahara et al. (2008), chondrule CH5 originated from a type C CAI-like refractory precursor, which was heated in the presence of precursors of ferromagnesian chondrules at a temperature much higher than 1300 °C, with dust/gas ratios 100 times the solar composition, and total pressure of 10^{-4} bar. Under these conditions, solid precursors would have evaporated except for Ca, Al-rich refractory precursors. During cooling below the temperature of 1300 °C, Mg and Si recondensed into the chondrule melt and forsterite crystallized. Mg-rich chondrules might be formed in the same environment. Bulk major element compositions in UOC chondrules show a significant Mg/Si elemental fractionation (Table 1). Nagahara et al. (2005) argue that the large Mg/Si fractionation seen from bulk major element compositions of ordinary chondrite chondrules is difficult to explain solely by

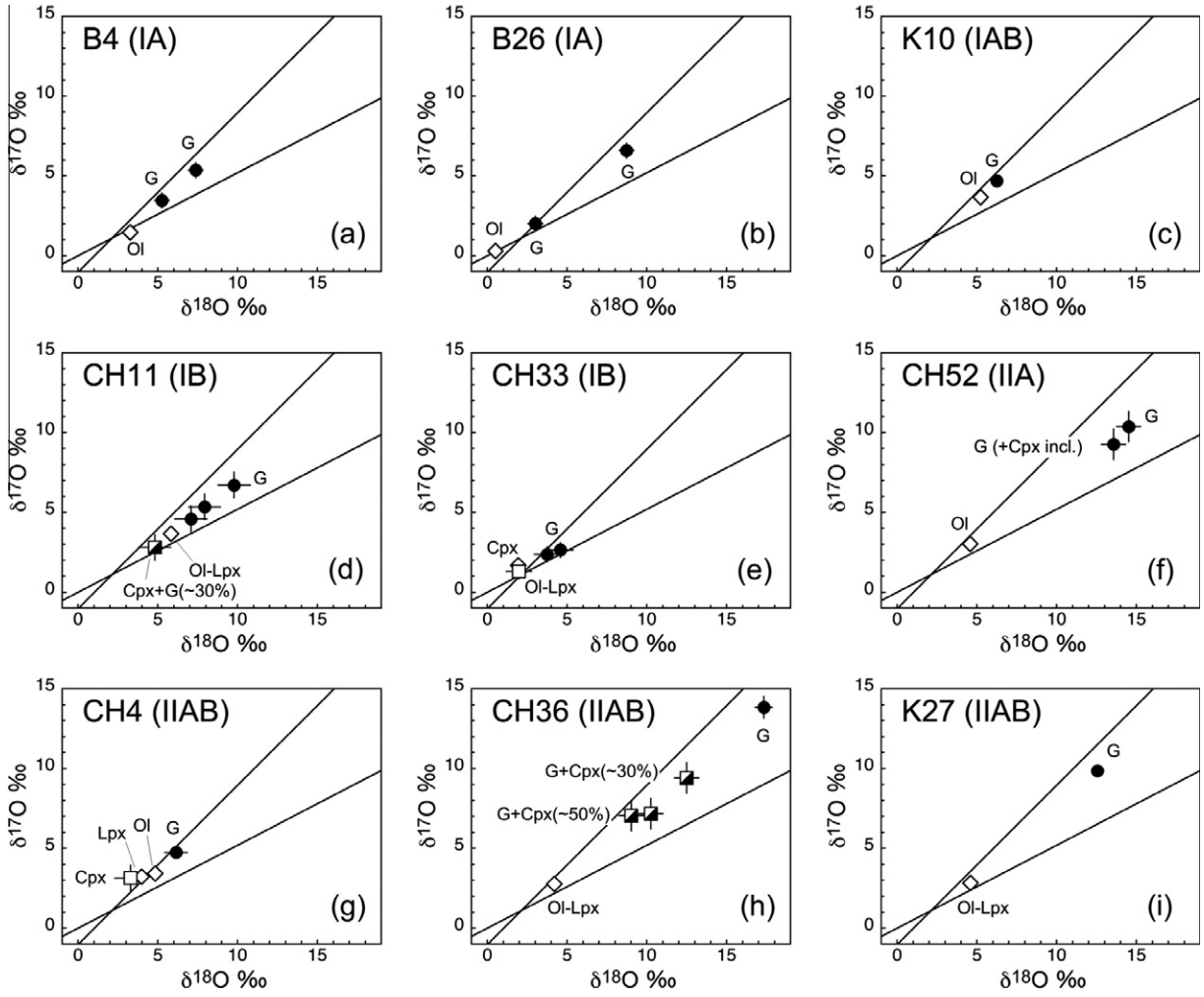

Fig. 9. The oxygen isotope ratios of mesostasis in selected chondrules. (a) B4, (b) B26, (c) K10, (d) CH11, (e) CH33, (f) CH52, (g) CH4, (h) CH36 and (i) K27. Data are shown in Table 4. In each plot, filled circles are glass, open squares are high Ca pyroxene (Cpx), open diamonds are olivine and low Ca pyroxene (Lpx) phenocryst data from 15 μm spot analysis and half filled squares are mixed analyses of overlapping glass and high Ca-pyroxene. The volume % of Cpx in the mixed analyses of Cpx-glass are shown in parentheses. Slope 1 and 0.5 lines represent the Y&R line and TF lines, respectively, shown as references.

condensation of solar composition gas, or by evaporation of chondritic precursors. In order to explain the observed major element fractionation among chondrules in ordinary chondrites, they proposed the fractionated solid precursors, which were depleted in refractory elements and metals, and the open system behavior of the major oxides by evaporation and recondensation during chondrule-forming melting events.

4.2.3. Equilibrium oxygen isotope fractionation under dust-enriched conditions

Clayton et al. (1991) mentioned that mass dependent fractionation of oxygen isotopes may occur between olivine and nebula gas at high temperature (~1500 °C), with the equilibrium fractionation factor $\Delta^{18}O(\text{olivine-}H_2O)$ of −2‰. According to a calculation by Onuma et al. (1972), both CO and H_2O molecules favor the heavy oxygen isotope compared to olivine at high temperature. To understand the mass dependent fractionation in oxygen isotopes among type I chondrules, we evaluate oxygen isotope fractionation between solid and gas at high temperature under dust-enriched conditions. We adapt the equilibrium condensation model in dust-enriched system by Ebel and Grossman (2000) to estimate fractionation of major elements and O-bearing molecules in solid and gas as a function of temperature. In the dust-enriched system, the composition of the gas changes with temperature and elemental composition of solid from which multiple gas species evaporates. In contrast to "solar nebula gas", which is of solar composition, a gas phase formed at high temperature in a dust-enriched system is referred to as "ambient gas" throughout the paper. We used one model parameter from Ebel and Grossman (2000) with a total pressure of 10^{-3} bar and dust enrichment of ×100 compared to solar compositions, which makes low FeO molar abundance in the silicate phases (mg# ~ 97) similar to type I chondrules. These parameters are similar to those used by Nagahara et al. (2008). We consider that carbon in the precursors

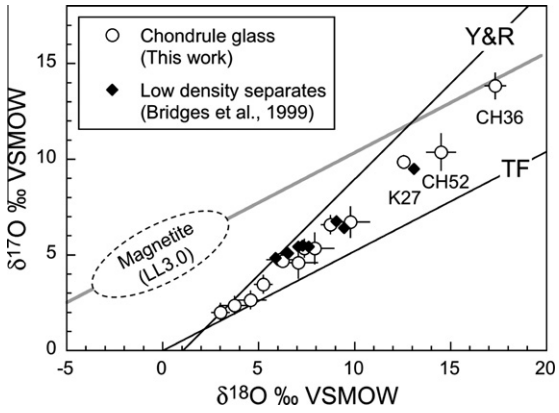

Fig. 10. Summary of oxygen three isotope ratios of glass in LL3.0–3.1 chondrules. The SIMS analyses of glass in this work are shown as open circles and low density separates from UOCs as filled diamonds (Bridges et al., 1999). The SIMS data plot along a single trend with the slope of ~0.8. The average oxygen isotope ratio of magnetite in matrix of Semarkona (Choi et al., 1998) is shown as comparison. Glass data from chondrule CH36 plot on the same mass fractionation line with magnetite data (gray line). Some chondrule glass data plot at the lower end of the trend and are close to those in olivine and pyroxene phenocrysts, indicating oxygen isotope exchange with aqueous fluid was insignificant in these chondrules.

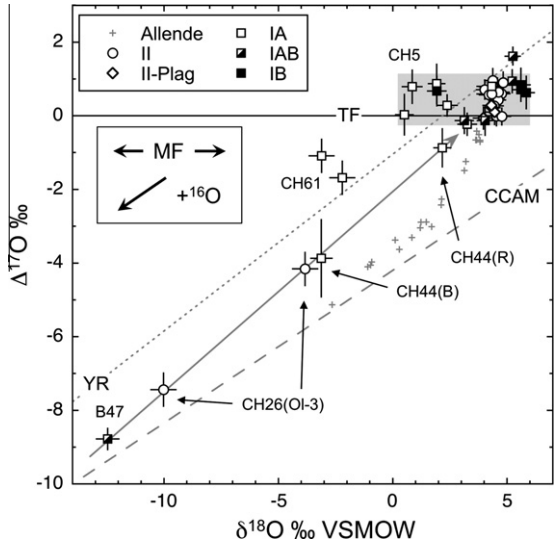

Fig. 11. The $\delta^{18}O$–$\Delta^{17}O$ plot of chondrules in LL3. The average olivine and pyroxene data are shown except for CH26 (olivine 3), CH44 blue and red CL olivine grains, and 2 analyses of olivine in CH61. Most of the data plot within a grey rectangle hatched area. In this diagram, a mass dependent isotope fractionation (MF) effect is seen as a spread of data horizontally with a constant $\Delta^{17}O$. TF, Y&R, and CCAM lines are shown as references. Grey crosses are bulk analyses of Allende CV3 chondrules (Clayton et al., 1983). The grey arrow shows a mixing trend between ^{16}O-rich component near CCAM line and the average chondrule values. The slope of the line is steeper than a simple enrichment or depletion of ^{16}O with the direction shown by the arrow labeled as "$+^{16}O$".

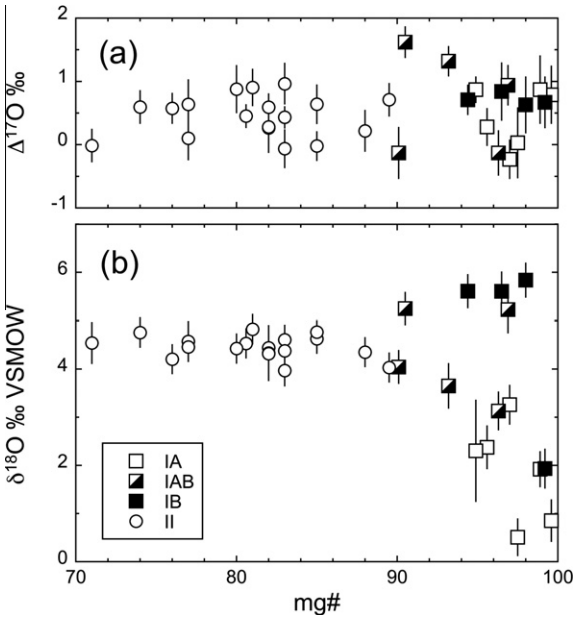

Fig. 12. The average oxygen isotope ratios of individual chondrules versus mg# of olivine and pyroxene. (a) $\Delta^{17}O$ and (b) $\delta^{18}O$. A large variation of $\delta^{18}O$ values are seen for mg# > 97, while $\Delta^{17}O$ values are indistinguishable.

produce CO and remaining oxygen atoms in gas produce H_2O at high temperature. Equilibrium oxygen isotope fractionation factors between silicate melt and molecules are estimated from reduced partition functions in the literature (Richet et al., 1977; Clayton and Kieffer, 1991) and shown in Table 5. In the calculation, we ignored the effect of SiO molecules in the gas by replacing them with H_2O molecules, because the reduced partition function of SiO molecule is not known. The reduced partition function of silicate is estimated as the average of those of olivine and diopside for simplicity. The calculation is done for the temperature range of 1177–1577 °C, where Mg and Si condense to solid. We define $\Delta^{18}O$ as fractionation of the $^{18}O/^{16}O$ ratio in solid and gas at high temperatures relative to the average precursor solid, but not the fractionation factor between solid and gas. It should be mentioned that O/Si and C/Si molar ratios of the system are nearly identical to those in the precursor dust when dust enriches more than 100 times the solar compositions. Therefore, the average oxygen isotope ratios in the system should be the same as that of average precursor dusts.

The results of the calculations are shown in Fig. 13b as a function of Mg/Si ratios of solid that change with the temperature of condensation. In the model by Ebel and Grossman (2000), they assumed "CI dust" that contains water (H_2O) and C at the level of bulk CI chondrites. Under these conditions, $\Delta^{18}O_{Solid}$ is nearly constant from −1.5‰ to −1.8‰ because more than a half of the oxygen in the system resides as H_2O molecules that buffer the isotope ratios of silicate. In comparison, two cases where precursor dusts are (1) anhydrous with carbon and (2) anhydrous and free of carbon are also calculated by simply reducing the O/Si atomic ratio from 7.8 to 3.6 for anhydrous dust and the C/Si atomic ratio from 0.85 to 0 for carbon-free dust.

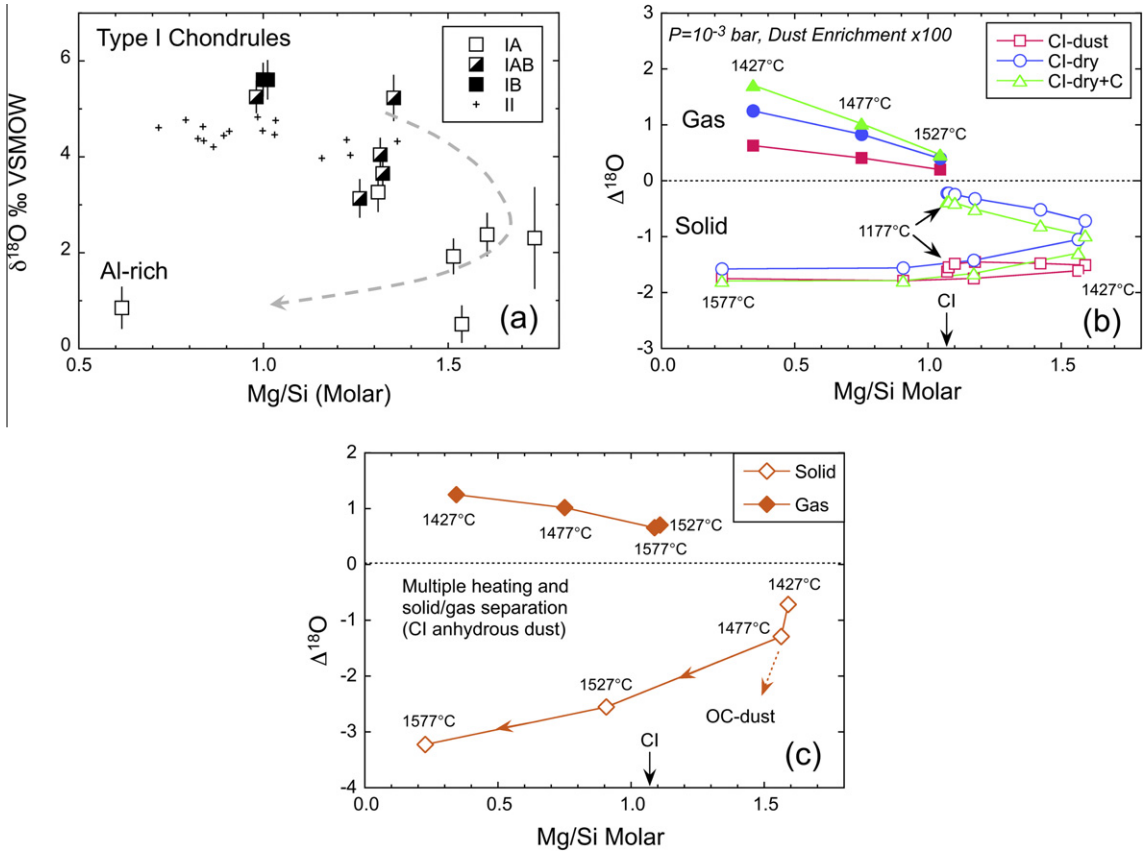

Fig. 13. The correlated Mg/Si ratios and oxygen isotope fractionations among type I chondrules. (a) Data from type I chondrules in this work. Grey crosses are data from type II chondrules. (b) Model oxygen isotope fractionation of chondrules under the dust enrichment of 100 times solar compositions with pressure of 10−3 bar. Major element compositions of solids are taken from Ebel and Grossman (2000). The $\Delta^{18}O$ is defined as the isotope fractionation of $\delta^{18}O$ in solid and gas from the initial average precursor solids. Calculations were made for three different precursors with different amounts of H_2O and C (see text). Open symbols are results of calculation for solid at temperatures from 1177 to 1577 °C. Filled symbols are isotope fractionation of gas at temperatures from 1427 to 1527 °C. The arrow labeled as "CI" represents the molar Mg/Si ratio of CI chondrites (Anders and Grevesse, 1989). (c) Model oxygen isotope fractionation during repeated evaporation and recondensation processes. Anhydrous CI-dust is assumed in the calculation. In this model, heating events occur four times at temperatures from $T = 1427$ to 1577 °C with 50 °C increments. Oxygen isotope fractionations in solid compared to initial ratios ($\Delta^{18}O$) are calculated for these temperature steps, which are shown as open diamonds. In the model, the gas phase enriched in heavy isotopes is removed at each step, which results in progressive depletion of $\delta^{18}O$ values. Oxygen isotope fractionations in the increment gas that are separated from solid are shown as filled diamonds. For OC-like precursors with the lower abundance of refractory elements (Al and Ca), Mg/Si ratios in solid may be higher than those for CI-dust precursors (Nagahara et al., 2005) as shown as a dashed-line arrow ("OC-dust").

The results of calculation with anhydrous precursors show decreasing $\Delta^{18}O_{solid}$ with increasing Mg/Si ratios of solid at a temperature lower than 1400 °C. This is a range of temperature where Mg condensed nearly 100%, while Si condensed only partially. With decreasing temperature, both Si and oxygen fully condensed to a solid, so that the oxygen isotope ratio does not change from the original values ($\Delta^{18}O_{solid} = 0$). At a higher temperature ($\geqslant$1500 °C), the major element composition is Ca, Al-rich with lower Mg/Si ratios and $\Delta^{18}O_{solid}$ is −1.8‰ in all cases, because oxygen in the system resides mainly in gas phases as H_2O.

The negative correlation between the $\delta^{18}O$ values and the Mg/Si ratios in type I chondrules (Fig. 13a) is similar to a result of the model calculation for anhydrous precursors. The Al-rich chondrule (CH5) shows both low $\delta^{18}O$ and lower Mg/Si, which is also shown in the model calculation at high temperature. However, differences in the $\delta^{18}O$ values between type IA chondrules and type IB chondrules are 3–5‰, much larger than those in the model calculation for the range of Mg/Si ratios. Therefore, equilibrium isotope fractionation between silicate and gas alone does not explain the observed range of $\delta^{18}O$ among type I chondrules. Additional fractionation could be caused by a kinetic fractionation during condensation (e.g., Richter, 2004), or by a high abundance of organic carbon in the precursor that formed abundant CO molecules in gas phase, though these effects may not be much larger than 1‰ level. It is also possible that the equilibrium fractionation of oxygen isotope between silicate and SiO molecule are much larger than that between silicate and H_2O molecule, which was used in the model calculation, though currently no data is available for SiO.

Here, we consider another model for the system with anhydrous CI-dust, in which the oxygen isotope

Table 5
Oxygen isotope fractionation between minerals (olivine and pyroxene) and gas (CO and H_2O) at high temperature.

T (°C)	Reduced partition function[a]				$\Delta^{18}O$ (solid–gas)[b]		
	CO $a = 18.202$ $b = -1.736$	H_2O $a = 15.624$ $b = -3.523$	Ol $a = 8.326$ $b = -0.142$ $c = 0.0032$	Px $a = 9.237$ $b = -0.199$ $c = 0.0053$	(Ol + Px)–CO (‰)	(Ol + Px)–H_2O (‰)	Ol–solar[c] (‰)
1900	3.78	3.15	1.76	1.95	−1.92	−1.30	−1.81
1800	4.14	3.44	1.93	2.14	−2.11	−1.41	−1.98
1700	4.56	3.78	2.13	2.36	−2.32	−1.54	−2.17
1600	5.05	4.17	2.36	2.62	−2.56	−1.68	−2.39
1500	5.61	4.61	2.63	2.92	−2.84	−1.84	−2.65
1400	6.28	5.13	2.96	3.28	−3.17	−2.02	−2.94
1300	7.07	5.78	3.34	3.70	−3.55	−2.26	−3.30
1200	8.02	6.45	3.81	4.22	−4.01	−2.44	−3.69
1100	9.16	7.27	4.38	4.84	−4.55	−2.66	−4.15
1000	10.57	8.30	5.08	5.63	−5.22	−2.94	−4.73
900	12.32	9.46	5.98	6.61	−6.03	−3.16	−5.39
800	14.49	10.94	7.13	7.88	−6.99	−3.44	−6.18

[a] $\ln(\beta) \times 1000 = aT^{-2} + bT^{-4} + cT^{-6}$, where T is absolute temperature (K). CO and H_2O molecules: the coefficients (a, b) of the equations are estimated from the theoretical calculations for 800, 900, 1100, and 1300 °C by Richet et al. (1977) with assuming $c = 0$. Olivine (Ol) and pyroxene (Px): coefficients (a, b, c) are from Clayton and Kieffer (1991).

[b] Equilibrium oxygen isotope fractionation between solid and gas, defined as $[\ln(\beta_{solid}) - \ln(\beta_{gas})] \times 1000‰$.

[c] "Solar" indicates the gas of solar system compositions, assuming 50% and 25% of oxygen atoms reside in CO and H_2O molecules, while rest of oxygen atoms are in silicate.

fractionation occurs by the multiple steps of the evaporation and recondensation processes. For the convenience of calculation, the model assumes that (1) the temperature of heating is 1427 °C for the first step and increases every 50 °C up to 1577 °C at the fourth step, (2) gas phase that is in oxygen isotope equilibrium with solid phase is removed from the system at each step, and (3) the major oxide composition at each temperature is adapted from the equilibrium condensation model of Ebel and Grossman (2000) with $P_{total} = 10^{-3}$ bar and dust enrichment of ×100 compared to solar compositions. Under these conditions, roughly a half of oxygen atoms reside in gas phase, which are enriched in $^{18}O/^{16}O$ and removed from the system at each step. The results of calculation show a progressive decrease in $\Delta^{18}O_{solid}$ by 0.6–1.2‰ at each step and a slight positive correlation between Mg/Si ratios and $\Delta^{18}O_{solid}$ (Fig. 13c). The $\Delta^{18}O_{solid}$ in the final solid at 1577 °C is as low as −3.2‰, and elemental compositions of the solid is similar to Al-rich chondrules with high Al and Ca abundance and subchondritic Mg/Si ratios. Therefore, this model may explain the results of Al-rich chondrule CH5, but not fully explains type IA chondrule B26 with low $\delta^{18}O$ and high Mg/Si (~1.5). The initial solid precursors of OC chondrules were likely to be depleted in refractory elements (i.e., lower Al and Ca) as indicated from bulk OC chondrite compositions. For the OC-chondritic initial dust compositions, compositional trajectory of condensed solid passes through higher Mg/Si ratios and lower Al and Ca abundances than those of CI-dust precursors (e.g., Nagahara et al., 2005). Therefore, the repeated heating processes for OC-dust would result in low $\Delta^{18}O_{solid}$ values with the Mg/Si ratios higher than that of CI dust, which are shown by dashed arrow in Fig. 13c and best explain the type IA data in Fig. 13a.

Incremental gas components separated from solid are also estimated and shown in Fig. 13c. The composition of gas in the first step (1427 °C) is too Si-rich compared to chondrules in LL3 chondrites. However, the Mg/Si ratios in the increment of gas separated from multiple heating steps gradually moves to that of CI-dust, while the $\Delta^{18}O_{gas}$ remains slightly positive (+0.7‰). The elemental compositions and isotope ratios of gas phase in this model match the chemical and isotopic signatures of type IB chondrule, i.e., subchondritic Mg/Si ratios (Fig. 13a), volatile element enrichment/refractory elements depletion (Fig. 1), and slightly elevated $\delta^{18}O$ values than the rest of chondrules by ~1‰ (Fig. 12). Thus, precursors of type IB chondrules may be fine-grained dusts that were condensed from fractionated gas. Consequently, common solid precursors for types IA and IB chondrules might have $\delta^{18}O$ values of ~5‰, slightly lower than those of IB (5.6–5.8‰).

In contrast to oxygen isotope fractionation among type I chondrules, significantly mass-dependent isotope fractionation in other elements (Mg, Si, K, Fe, and S) have not been observed previously (e.g., Alexander et al., 2000; Alexander and Wang, 2001; Yu et al., 2003; Tachibana and Huss, 2005). Equilibrium isotope fractionations of Mg and Si between gas species and silicates are much smaller (e.g., Mg atoms and SiO molecules versus Mg and Si in olivine) than the case for oxygen isotope, so that significant mass fractionation of Mg and Si isotopes may not be expected.

4.2.4. Apparent closed system for type II chondrules

The equilibrium condensation model by Ebel and Grossman (2000) explains high FeO contents of type II chondrules by heating of "CI dust" that was enriched more than ×1000 of solar compositions. The model calculations of the oxygen isotope fractionations between gas and silicates under the dust enrichment of ×1000 compared to solar compositions are also performed and shown in Fig. EA9. The condensation temperatures of Mg and Si

under such conditions become much higher (1500–1700 °C), indicating that major element fractionation may occur only at temperatures much higher than 1500 °C. Assuming the "CI dust" as precursor, the system produces a significant amount of H_2O evaporated from water ice. Then, the $\delta^{18}O$ values in silicates decrease by ~1‰ as a result of fractionation between silicate and H_2O. If precursor dusts were anhydrous, even with high enrichment of dust at ×1000 of solar compositions, high FeO contents of type II chondrules (i.e., mg# between 90 and 70) may not be explained due to low oxygen fugacity in the gas (Fedkin and Grossman, 2006). If a small amount of water ice, for example at the level of 1 wt% (one-tenth of that in CI chondrites ~10 wt%), dust enrichment of ~10,000 times the solar compositions may be required to reproduce FeO contents in type II chondrules. In this case, oxygen isotope fractionation in silicates should be small (⩽0.2‰) unless precursors were heated to a high temperature above condensation of major oxides (MgO and SiO_2). Small variations in $\delta^{18}O$ values among type II chondrules are consistent with either constant fractionation from CI dust precursor, or nearly no fractionation with anhydrous dust precursors. If the $\delta^{18}O$ values in type II chondrules reflect fractionation between silicates and water in gas during chondrule formation, the $\delta^{18}O$ value of the average precursor "CI dust" should be ~1‰ higher in $\delta^{18}O$, which is similar to those of type IB chondrules with $\delta^{18}O$ of 5.5–6.0‰.

In the above conditions to form type II chondrules, a mole fraction of H_2O (i.e., ~molar H_2O/H_2) would be as high as ~0.2 with either "CI dust" with the enrichment of ×1000 of solar compositions, or dust containing 1 wt% water-ice with the enrichment of ×10,000. This value is orders of magnitude higher than estimates for the solar nebula ($\sim 5 \times 10^{-4}$). Oxygen isotope exchange experiments between the melt and H_2O vapor, Yu et al. (1995) indicate that multiple melting events might be required to highly exchange oxygen isotopes with nebula gas due to low gas density. Under the conditions with high enrichment of dust and existence of water ice, nearly complete oxygen isotope exchange between ambient gas and chondrule melt might occur. Thus, type II chondrule formation would result in nearly homogeneous oxygen isotope ratios among minerals within a chondrule, as well as among chondrules forming in the same environment. This is consistent with the narrow range of oxygen isotope ratios observed from type II chondrules in this study.

4.3. Link to chondrules in carbonaceous chondrites

The lowest $\Delta^{17}O$ value among all the chondrules analyzed in this study is obtained from a type IAB chondrule; -8.8 ± 0.3‰ in B47. It is likely that the precursor solids of chondrules in LL were initially heterogeneous in oxygen three isotopes with variable degrees of ^{16}O-enrichments, similar to the case of chondrules in carbonaceous chondrites. The oxygen isotope ratios from three ^{16}O-rich chondrules (CH26, CH44, and B47) plot towards the CCAM line (Figs. 4b and 11), similar to those of chondrules in CV (e.g., Clayton et al., 1983; Jones et al., 2004). These data strongly indicate that chondrules in LL3 share the common oxygen isotope reservoir with chondrules in carbonaceous chondrites. The oxygen isotope analyses of Al-rich chondrules in UOCs show similar negative $\Delta^{17}O$ values down to −6‰, but plot nearly on the Y&R line (Russell et al., 2000), though these data could not be resolved from the CCAM line due to relatively large analytical uncertainties (~2–3‰) of earlier SIMS analyses. Data from chondrule CH61 (type IA) in this work plot slightly above the Y&R line, similar to those of Al-rich chondrules. It is possible some IA and Al-rich chondrules started from refractory precursors that had oxygen isotope ratios on a linear trend made by B47, CH26, and CH44, and their oxygen isotope ratios are mass fractionated towards lower $\delta^{18}O$ by an extensive evaporation and recondensation process during chondrule formation.

As shown in Fig. 14, the BO chondrule data from CV3 chondrites deviate significantly from the CCAM line in the oxygen three isotope diagram with a steeper slope towards bulk OC chondrule data (Clayton et al., 1983, 1991). Clayton et al. (1983) considered oxygen isotope ratios in BO chondrules in Allende CV3 to represent that of nebula gas, because BO chondrules formed by complete melting of the solid precursor. A similar conclusion was made from the SIMS analyses of chondrules in CV3 and CR2 by Chaussidon et al. (2008), who estimated the oxygen isotope ratios in the solar nebular gas to be on the TF line with $\delta^{18}O = 3.6 \pm 1$‰ and $\delta^{17}O = 1.8 \pm 1$‰. They further indicated chondrules from UOC and EH chondrites, also formed in the nebula gas with the identical oxygen isotope ratios. The majority of chondrules analyzed in this work, especially type II chondrules, also plot along the extension of CV3 BO chondrule data (see Figs. 4c and 14), so that these chondrules from two different chondrite groups might share a common isotope reservoir during their formation.

Clayton et al. (1991) presented a model for partial isotope exchange between ^{16}O-rich solid and ^{16}O-poor nebula gas that differ in $\Delta^{17}O$ at the level of a few ‰, similar to the level of equilibrium isotope fractionation between solid and H_2O gas at high temperature (Fig. 8 of Clayton et al., 1991). The mixing line forms a slope much steeper than unity, similar to the trend between CV3 BO chondrules and K25 in Fig. 14. However, as we discussed in the previous section, oxygen isotope ratios of type II chondrules might be very similar to the average of solid precursors (including ice if present) due to a significant enrichments of dust compared to the solar compositions. Therefore, contribution from the nebula gas should be very small. Alternatively, a linear trend in Fig. 14 could be a mixing line between two solid precursors, represented by K25 (IAB) and BO chondrules in CV3 (Fig. 14), respectively. The ^{16}O-poor precursor, similar to K25, might experience a large oxygen isotope fractionation between solid and gas, as has been proposed for type IA chondrule formation. Furthermore, before chondrules started to form in the local disk regions, heating of disk material under low dust concentrations might also cause a large isotope fractionation in solid phases. As an extreme case, the equilibrium isotope fractionation between olivine and solar nebula under the standard solar nebula compositions (no dust enrichment) is estimated to be −4‰ at the condensation temperature

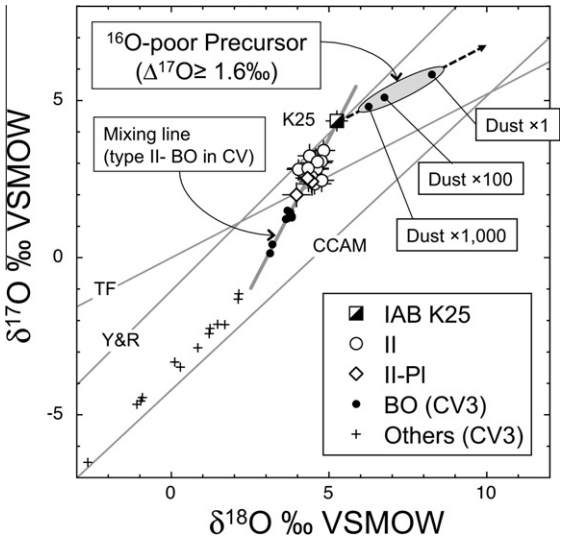

Fig. 14. The oxygen isotope mixing trend among type II chondrules in LL3 and BO chondrules in CV3. Data from K25 (IAB) and type II chondrules are from this work. Data from BO and porphyritic (labeled as "others") chondrules in CV3 are from Clayton et al. (1983). TF, Y&R, and CCAM lines are shown as references. A solid grey line is the mixing line between K25 and BO chondrules in CV3, on which most type II chondrules plot. Assuming the oxygen isotope ratios in K25 to be the ^{16}O-poor end member, those in the ^{16}O-poor precursors are estimated from which oxygen isotope ratios in solid were fractionated. The estimated range of precursors is shown as a grey oval area, where "Dust × 1", "Dust × 100", and "Dust × 1000" represent enrichments of dust relative to solar compositions. Multiple heating events affecting the precursors, such as repeated chondrule formation, would result in larger isotope fractionation, so that the initial oxygen isotope reservoir of the LL chondrite forming regions could be along the mass dependent fractionation line shown by the dashed arrow.

of olivine (~1170 °C; Yoneda and Grossman, 1995, see Table 5). Considering the mass balance of oxygen between solid and gas, the average oxygen isotope ratios of gas and solid would be 3‰ higher in δ^{18}O along the same mass fractionation line (Fig. 14, "Dust × 1"). Therefore, if precursor solids in LL chondrites formed in equilibrium with the local solar nebula, the oxygen isotope ratios of the gas would have been heavier in δ^{18}O compared to that of K25, as shown in Fig. 14.

4.4. Internal oxygen isotope heterogeneity within a chondrule

4.4.1. Case for ^{16}O-poor relict grains and ^{16}O-rich overgrowths

As described earlier, CH44 shows reversed zoning in olivine phenocrysts, $Fo_{99.3}$ core overgrown by $Fo_{99.7}$ rim. The resorption texture of zoned olivine is clearly seen in the CL image (Fig. 6a) and indicates that the olivine core is an unmelted relict, and the reverse zoning of olivine overgrowth resulted from disequilibrium between the olivine core and the melt. The most interesting feature in CH44 is that the relict olivines show slightly FeO-rich ($Fo_{99.3}$) compositions and higher Δ^{17}O values ~−0.8‰ than overgrowths ($Fo_{99.7}$, $\Delta^{17}O = -4‰$). This is different from the normal occurrence of relict grains that are usually more Mg-rich and ^{16}O-rich (e.g., Kunihiro et al., 2004, 2005; Jones et al., 2004). The oxygen isotope data from two types of olivine seem to plot on the mixing line between B47 and majority of other chondrules (Fig. 11).

One interpretation is that CH44 formed in the carbonaceous chondrite-forming region with ^{16}O-rich ambient gas, whereas the precursor solid included grains derived from the ordinary chondrite-forming region. However, as we discussed above, the precursor of ordinary chondrites might include ^{16}O-rich refractory components, so that CH44 might have formed in the ordinary chondrite region from two solid precursors, one with refractory-rich and ^{16}O-rich components, and another with large forsterite grains ($\geqslant$100 μm) and relatively ^{16}O-poor oxygen isotope ratios. The systematic differences in Ca and Al contents in the two types of olivine support the hypothesis that the olivine overgrowths crystallized in a melt with high refractory element abundance. According to Pack et al. (2004), refractory forsterite (RF) grains with bright CL are found in various types of chondritic meteorites and their oxygen isotope ratios are consistently ^{16}O-rich compared to other olivine grains in the same meteorites. It seems likely that refractory-rich precursors in CH44 share similar chemical and isotope characteristics with those of precursors of RF in other chondrites. Moderately ^{16}O-rich isotope ratios ($\Delta^{17}O = -4‰$) in glass and melt-grown olivine in CH44 are likely in the equilibrium with the ambient gas, which might have the intermediate Δ^{17}O value by averaging ^{16}O-rich ($\Delta^{17}O \leqslant -6‰$) and ^{16}O-poor ($\Delta^{17}O \sim 0‰$) precursors.

4.4.2. Origin of relict olivine grains in chondrules

In addition to CH44 discussed above, only one type II chondrule showed a relict olivine with the oxygen isotope ratios significantly below the TF line (CH26, IIAB; Fig. 4b). It seems that chondrules in LL3 are more internally homogeneous than chondrules in other groups of chondrites, such as CV (Jones et al., 2004; Chaussidon et al., 2008), CO (Kunihiro et al., 2004), Acfer 094 ungrouped C (Kunihiro et al., 2005; Ushikubo et al., 2009), and Y-793408 H3.2 (Kita et al., 2008), in which ^{16}O-rich relict olivine are more frequently observed. With the improved analytical precision, several chondrules that were examined in this work show internal oxygen isotope heterogeneity at the level of a few ‰, as shown in Fig. 7. These chondrules are mainly from FeO-poor porphyritic chondrules showing a hint of incomplete melting, such as dusty olivine grains and large phenocrysts. The heterogeneous oxygen isotope ratios observed among these chondrules completely overlap with those of internally homogeneous chondrules (Fig. 4c). Therefore, the origin of relict grains is most likely from fragments of chondrules that were incorporated among the precursors of newly formed chondrules.

Libourel and Krot (2007) suggested a planetary origin for relict olivine grains in type I chondrules based on granoblastic chondrules in CV3. They considered that a large systematic difference in the oxygen isotope ratios of olivine and pyroxene would support their hypothesis, This difference was not found for the chondrules we report in this paper.

4.5. Relationship between oxygen isotopes and Al–Mg ages of LL3 chondrules

In type II chondrules from LL3.0–3.1 chondrites, the ^{26}Al–^{26}Mg ages correlate with the enrichment of Si relative to Mg (Mostefaoui et al., 2002; Tachibana et al., 2003; Tomomura et al., 2004; Kita et al., 2005). Tachibana et al. (2003) suggested that the Si/Mg ratios of chondrule precursors in UOC-forming regions changed with time as a result of repeated chondrule formation associated with evaporation and recondensation of elements that are more volatile than Mg. In contrast, the oxygen isotope ratios in type II chondrules fall in a narrow range and do not show any correlation with bulk chondrule Si/Mg ratios. As discussed above, it is likely that oxygen isotope ratios of type II chondrule precursors were homogenized in dust-rich environments.

In three type IIAB chondrules (CH4, CH36 and K27), both the initial $^{26}Al/^{27}Al$ ratios and oxygen three isotope ratios were obtained for the glass. The initial $^{26}Al/^{27}Al$ ratios in CH36 and K27 are $(6.6 \pm 1.9) \times 10^{-6}$ and $(6.1 \pm 1.7) \times 10^{-6}$, respectively, which are lower than that of CH4, $(9.0 \pm 1.6) \times 10^{-6}$. As shown in Figs. 9 and 10, glass in CH36 and K27 yields high $\Delta^{17}O$ values of 3–5‰, indicating that oxygen isotopes exchanged with an aqueous phase during parent body metamorphism. In contrast, the Al–Mg isotope system of these chondrules does not show any evidence of later disturbance (Kita et al., 2000, 2005). Correlated ^{26}Mg excesses with Al/Mg ratios are observed from glass analyses in both CH4 and CH36 (Kita et al., 2000). A similar range of inferred initial $^{26}Al/^{27}Al$ ratios of $(7–10) \times 10^{-6}$ are obtained from plagioclase-bearing type II chondrules (Kita et al., 2000; Mostefaoui et al., 2002; Kita et al., 2005), so that there is no difference between the Al–Mg data obtained from glass analyses and from anorthitic plagioclase analyses. These data also argue against redistribution of Al and Mg in glass that exchanged oxygen isotopes with aqueous fluid.

It is perplexing that oxygen isotope exchange with aqueous fluid occurred without Mg isotope diffusion in the same glass. Due to a lack of low temperature diffusion experiments, it is not possible to compare isotope diffusion rates between oxygen and Mg in hydrated glass. In order to disturb the Al–Mg system, Mg isotope exchange should occur between glass and other Mg-rich phases, most likely Ca-pyroxene microcrystallites. If Mg isotope diffusion in Ca pyroxene was very slow during parent body thermal metamorphism, Mg with normal isotope ratios might not be available for isotope exchange with glass. Further studies comparing oxygen isotopes and Mg isotopes in glass may address this question.

5. CONCLUSIONS

We have performed a systematic examination of 36 chondrules from some of the least equilibrated ordinary chondrites using newly developed very precise and accurate (sub-‰) SIMS oxygen three-isotope analyses. These high precision analyses are able to resolve mass dependent oxygen isotope fractionations that are superimposed on mass independent isotope effects in ferromagnesian chondrules. Bulk types IA and IB chondrules show mass dependent fractionations of ~5‰ in $\delta^{18}O$, where refractory element-rich type IA chondrules are enriched in the light isotopes and volatile element-rich type IB chondrules are slightly enriched in the heavy isotopes. This is the first study to correlate isotopic fractionation with chemistry and mineralogy of chondrules in ordinary chondrites. In contrast, oxygen isotope ratios in type II chondrules have a limited range with an average $\delta^{18}O$ of 4.51 ± 0.44‰, $\delta^{17}O = 2.89 \pm 0.60$‰, and $\Delta^{17}O = 0.54 \pm 0.60$‰, (2SD, $n = 14$), which is slightly enriched in ^{16}O relative to bulk LL chondrites.

The systematic differences in oxygen isotope ratios among different types of chondrules may be explained by variable enrichment of dust during chondrule-forming heating events. At lower levels of dust enrichment (dust/gas ratios at 100 times solar), evaporation and recondensation of solids may result in oxygen isotope fractionation between chondrule melt and gas, which accompanies bulk Mg/Si fractionation. Thus, the isotopic and chemical characteristics of type IA chondrules may be explained by recondensation of major oxides and separation of gas and solid, similar to the process proposed for Al-rich glassy chondrules by Nagahara et al. (2008). Type II chondrule data are best explained by the formation from precursors with a small amount of water ice (e.g., 1/10 of CI chondrites) under the higher dust enrichment (1000–10,000 times solar). Evaporation and recondensation of major oxides are suppressed so that oxygen isotope fractionations in solid did not occur significantly. With a higher water partial pressure in the ambient gas, which resulted in high FeO abundance of type II chondrules, oxygen isotope ratios among type II chondrules might be homogenized by isotope exchange with water vapor in the ambient gas.

Data from chondrule glasses show a large variation in $\delta^{18}O$ and $\delta^{17}O$, up to 17‰ and 14‰ in CH36 (type IIAB), respectively, and form a linear trend with the slope of 0.8. The highest chondrule glass $\Delta^{17}O$ value of 4.8 ± 0.7‰ in Semarkona is consistent with the magnetite $\Delta^{17}O$ values in Semarkona (Choi et al., 1998), indicating that oxygen isotopes in glass exchanged with an aqueous fluid in the LL parent body. The data from olivine and pyroxene suggest that the precursors of chondrules in ordinary chondrites were made of both ^{16}O-poor precursors ($\Delta^{17}O \geqslant 1.6$‰) and the ^{16}O-rich precursors ($\Delta^{17}O$ as low as -9‰) common to chondrules in carbonaceous chondrites. Depending on the chondrule heating conditions, mixing of these two reservoirs occurred in various proportions during melting of chondrules and through the isotope exchange between ambient gas and chondrule melt. Further studies using high precision SIMS oxygen isotope analyses of chondrules from various chondrite groups may help us to understand the variety of isotope reservoirs and physical conditions during formation of chondrules in the proto-planetary disk.

ACKNOWLEDGMENTS

We appreciate loans of thin sections of Semarkona (Glenn MacPherson and Timothy McCoy, Smithsonian Institution) and Bishunpur and Krymka (Franz Brandstütter and Gero Kürat,

Natural History Museum, Vienna). We thank Klaus P. Jochum for providing MPI-DING glass standards. We thank Brian Hess for preparation of oxygen isotope standard mounts, Bin Fu for assisting with SIMS analyses of some standard mounts, and Jim Kern for technical support. Critical comments from Conel Alexander, Marc Chaussidon, Hisayoshi Yurimoto, and Sasha Krot improved the quality of the manuscript significantly. Takayuki Ushikubo, Kazuhito Ozawa, Makoto Kimura, Daisuke Nakashima, Rudraswami Gowda, and Mike Weisberg are acknowledged for helpful discussions. This work is supported by NASA Cosmochemistry Program (NNX07AI46G, N.K.). WiscSIMS is partly supported by NSF (EAR03-19230, EAR05-16725, EAR07-44079).

APPENDIX A. SUPPLEMENTARY DATA

Supplementary data associated with this article can be found, in the online version, at doi:10.1016/j.gca.2010.08.011.

REFERENCES

Alexander C. M. O. and Wang J. (2001) Iron isotopes in chondrules: implications for the role of evaporation during chondrule formation. *Meteorit. Planet. Sci.* **36**, 419–428.

Alexander C. M. O. and Grossman J. N. (2005) Alkali elemental and potassium isotopic compositions of Semarkona chondrules. *Meteorit. Planet. Sci.* **40**, 541–556.

Alexander C. M. O., Barber D. J. and Hutchison R. (1989) The microstructure of Semarkona and Bishunpur. *Geochim. Cosmochim. Acta* **53**, 3045–3057.

Alexander C. M. O., Grossman J. N., Wang J., Zanda B., Bourot-Denise M. and Hewins R. H. (2000) The lack of potassium-isotopic fractionation in Bishunpur chondrules. *Meteorit. Planet. Sci.* **35**, 859–868.

Alexander C. M. O., Grossman J. N., Ebel D. S. and Ciesla F. J. (2008) The formation conditions of chondrules and chondrites. *Science* **320**, 1617–1619.

Amelin Y., Krot A. N., Hutcheon I. D. and Ulyanov A. A. (2002) Lead isotopic ages of chondrules and calcium–aluminum-rich inclusions. *Science* **297**, 1678–1683.

Anders E. and Grevesse N. (1989) Abundances of the elements – meteoritic and solar. *Geochim. Cosmochim. Acta* **53**, 197–214.

Behrens H., Zhang Y. X., Leschik M., Wiedenbeck M., Heide G. and Frischat G. H. (2007) Molecular H_2O as carrier for oxygen diffusion in hydrous silicate melts. *Earth Planet. Sci. Lett.* **254**, 69–76.

Behrens H., Zhang Y. X. and Xu Z. G. (2004) H_2O diffusion in dacitic and andesitic melts. *Geochim. Cosmochim. Acta* **68**, 5139–5160.

Boesenberg J. S., Young E. D., Ziegler K. and Hewins R. H. (2005) Evaporation and the absence of oxygen isotopic exchange between silicate melt and carbon monoxide gas at nebular pressures. *Meteorit. Planet. Sci. Suppl.* **40**, A22.

Bridges J. C., Franchi I. A., Hutchison R., Sexton A. S. and Pillinger C. T. (1998) Correlated mineralogy, chemical compositions, oxygen isotopic compositions and size of chondrules. *Earth Planet. Sci. Lett.* **155**, 183–196.

Bridges J. C., Franchi I. A., Sexton A. S. and Pillinger C. T. (1999) Mineralogical controls on the oxygen isotopic compositions of UOCs. *Geochim. Cosmochim. Acta* **63**, 945–951.

Chaussidon M., Libourel G. and Krot A. N. (2008) Oxygen isotopic constraints on the origin of magnesian chondrules and on the gaseous reservoirs in the early Solar System. *Geochim. Cosmochim. Acta* **72**, 1924–1938.

Choi B. G., McKeegan K. D., Leshin L. A. and Wasson J. T. (1997) Origin of magnetite in oxidized CV chondrites: in situ measurement of oxygen isotope compositions of Allende magnetite and olivine. *Earth Planet. Sci. Lett.* **146**, 337–349.

Choi B. G., McKeegan K. D., Krot A. N. and Wasson J. T. (1998) Extreme oxygen-isotope compositions in magnetite from unequilibrated ordinary chondrites. *Nature* **392**, 577–579.

Ciesla F. J. (2005) Chondrule-forming processes – an overview. In *Chondrites and the Protoplanetary Disk*, vol. 341 (eds. A. N. Krot, E. R. Scott and B. Reipurth). Astronomical Society of the Pacific Conference Series, pp. 811–820.

Clayton R. N. (1993) Oxygen isotopes in meteorites. *Annu. Rev. Earth Planet. Sci.* **21**, 115–149.

Clayton R. N. (2002) Self-shielding in the solar nebula. *Nature* **415**, 860–861.

Clayton R. N. and Kieffer S. W. (1991) Oxygen isotopic thermometer calibrations. In *Stable Isotope Geochemistry: A Tribute to Samuel Epstein* (eds. H. P. Taylor Jr., J. R. O'Neil and I. R. Kaplan). Geochim. Soc. Spec. Publ. 3, pp. 3–10.

Clayton R. N. and Mayeda T. K. (1999) Oxygen isotope studies of carbonaceous chondrites. *Geochim. Cosmochim. Acta* **63**, 2089–2104.

Clayton R. N., Grossman L. and Mayeda T. K. (1973) Component of primitive nuclear composition in carbonaceous meteorites. *Science* **182**, 485–488.

Clayton R. N., Onuma N., Grossman L. and Mayeda T. K. (1977) Distribution of pre-solar component in Allende and other carbonaceous chondrites. *Earth Planet. Sci. Lett.* **34**, 209–224.

Clayton R. N., Onuma N., Ikeda Y., Mayeda T. K., Hutcheon I. D., Olsen E. J. and Molini-Velsko C. (1983) Oxygen isotopic compositions of chondrules in Allende and ordinary chondrites. In *Chondrules and their Origins* (ed. E. A. King). Lunar Planet. Inst., Houston, pp. 37–43.

Clayton R. N., Mayeda T. K., Goswami J. N. and Olsen E. J. (1991) Oxygen isotope studies of ordinary chondrites. *Geochim. Cosmochim. Acta* **55**, 2317–2337.

Connolly H. C. and Love S. G. (1998) The formation of chondrules: petrologic tests of the shock wave model. *Science* **280**, 62–67.

Downes H., Mittlefehldt D. W., Kita N. T. and Valley J. W. (2008) Evidence from polymict ureilite meteorites for a disrupted and re-accreted single ureilite parent asteroid gardened by several distinct impactors. *Geochim. Cosmochim. Acta* **72**, 4825–4844.

Ebel D. S. and Grossman L. (2000) Condensation in dust-enriched systems. *Geochim. Cosmochim. Acta* **64**, 339–366.

Fedkin A. V. and Grossman L. (2006) The fayalite content of chondritic olivine: obstacle to understanding the condensation of rocky material. In *Meteorites and the Early Solar System II* (eds. D. S. Lauretta and H. Y. McSween Jr.). University of Arizona Press, Tucson, pp. 279–294.

Gaidos E., Krot A. N. and Huss G. R. (2009) On the oxygen isotopic composition of the solar system. *Astrophys. J.* **705**, L163–L167.

Gounelle M., Krot A. N., Nagashima K. and Kearsley A. (2009) Extreme ^{16}O enrichment in calcium–aluminum-rich inclusions from the Isheyevo (CH/CB) chondrite. *Astrophys. J.* **698**, L18–L22.

Greshake A. (1997) The primitive matrix components of the unique carbonaceous chondrite Acfer 094: a TEM study. *Geochim. Cosmochim. Acta* **61**, 437–452.

Grossman J. N. (1988) Formation of chondrules. In *Meteorites and the Early Solar System* (eds. J. F. Kerridge and M. S. Mathews). University of Arizona Press, Tucson, pp. 680–696.

Grossman J. N. and Wasson J. T. (1983) Refractory precursor components of Semarkona chondrules and the fractionation of

refractory elements among chondrites. *Geochim. Cosmochim. Acta* **47**, 759–771.

Grossman J. N. and Wasson J. T. (1987) Compositional evidence regarding the origins of rims on Semarkona chondrules. *Geochim. Cosmochim. Acta* **51**, 3003–3011.

Grossman J. N. and Brearley A. J. (2005) The onset of metamorphism in ordinary and carbonaceous chondrites. *Meteorit. Planet. Sci.* **40**, 87–122.

Grossman J. N., Alexander C. M. O., Wang J. H. and Brearley A. J. (2000) Bleached chondrules: evidence for widespread aqueous processes on the parent asteroids of ordinary chondrites. *Meteorit. Planet. Sci.* **35**, 467–486.

Grossman J. N., Alexander C. M. O., Wang J. H. and Brearley A. J. (2002) Zoned chondrules in Semarkona: evidence for high- and low-temperature processing. *Meteorit. Planet. Sci.* **37**, 49–73.

Guan Y., McKeegan K. D. and MacPherson G. J. (2000) Oxygen isotopes in calcium, aluminum-rich inclusions from enstatite chondrites: new evidence for a common CAI source in solar nebula. *Earth Planet. Sci. Lett.* **181**, 271–277.

Heck P. R., Ushikubo T., Schmitz B., Kita N. T., Spicuzza M. J. and Valley J. W. (2010) A single asteroidal source for extraterrestrial Ordovician chromite grains from Sweden and China: high-precision oxygen three-isotope SIMS analysis. *Geochim. Cosmochim. Acta* **74**, 497–509.

Hiyagon H. and Hashimoto A. (1999) ^{16}O excesses in olivine inclusions in Yamato86009 and Murchison chondrites and their relation to CAIs. *Science* **283**, 828–831.

Hutcheon I. D. and Hutchison R. (1989) Evidence from the Semarkona ordinary chondrite for Al-26 heating of small planets. *Nature* **337**, 238–241.

Jarosewich E. (1990) Chemical analyses of meteorites – a compilation of stony and iron meteorite analyses. *Meteoritics* **25**, 323–337.

Jochum K. P., Stoll B., Herwig K., Willbold M., Hofmann A. W., Amini M., Aarburg S., Abouchami W., Hellebrand E., Mocek B., Raczek I., Stracke A., Alard O., Bouman C., Becker S., Ducking M., Bratz H., Klemd R., de Bruin D., Canil D., Cornell D., de Hoog C. J., Dalpe C., Danyushevsky L., Eisenhauer A., Gao Y. J., Snow J. E., Goschopf N., Gunther D., Latkoczy C., Guillong M., Hauri E. H., Hofer H. E., Lahaye Y., Horz K., Jacob D. E., Kassemann S. A., Kent A. J. R., Ludwig T., Zack T., Mason P. R. D., Meixner A., Rosner M., Misawa K. J., Nash B. P., Pfander J., Premo W. R., Sun W. D., Tiepolo M., Vannucci R., Vennemann T., Wayne D. and Woodhead J. D. (2006) MPI-ding reference glasses for in situ microanalysis: new reference values for element concentrations and isotope ratios. *Geochem. Geophys. Geosyst.* **7**, 44.

Jones R. H. (1990) Petrology and mineralogy of type-II, FeO-rich chondrules in Semarkona (LL3.0) – origin by closed-system fractional crystallization, with evidence for supercooling. *Geochim. Cosmochim. Acta* **54**, 1785–1802.

Jones R. H. (1994) Petrology of FeO-poor, porphyritic pyroxene chondrules in the Semarkona chondrite. *Geochim. Cosmochim. Acta* **58**, 5325–5340.

Jones R. H. (1996) FeO-rich, porphyritic pyroxene chondrules in unequilibrated ordinary chondrites. *Geochim. Cosmochim. Acta* **60**, 3115–3138.

Jones R. H. and Scott E. R. D. (1989) Petrology and thermal history of type IA chondrules in the Semarkona (LL3.0) chondrite. In *Proceedings of the 19th Lunar and Planetary Science Conference*, pp. 523–536.

Jones R. H., Leshin L. A., Guan Y. B., Sharp Z. D., Durakiewicz T. and Schilk A. J. (2004) Oxygen isotope heterogeneity in chondrules from the Mokoia CV3 carbonaceous chondrite. *Geochim. Cosmochim. Acta* **68**, 3423–3438.

Jones R. H., Grossman J. N. and Rubin A. E. (2005) Chemical, mineralogical and isotopic properties of chondrules: clues to their origin. In *Chondrites and the Protoplanetary Disk*, vol. 341 (eds. A. N. Krot, E. R. Scott and B. Reipurth). Astronomical Society of the Pacific Conference Series, pp. 251–285.

Kita N. T., Nagahara H., Togashi S. and Morishita Y. (2000) A short duration of chondrule formation in the solar nebula: evidence from ^{26}Al in Semarkona ferromagnesian chondrules. *Geochim. Cosmochim. Acta* **64**(22), 3913–3922.

Kita N. T., Ikeda Y., Togashi S., Liu Y., Morishita Y. and Weisberg M. K. (2004) Origin of ureilites inferred from a SIMS oxygen isotopic and trace element study of clasts in the Dar al Gani 319 polymict ureilite. *Geochim. Cosmochim. Acta* **68**(20), 4213–4235.

Kita N. T., Tomomura S., Tachibana S., Nagahara H., Mostefaoui S. and Morishita Y. (2005) Correlation between aluminum-26 ages and bulk Si/Mg ratios for chondrules from LL3.0–3.1 chondrites. *Lunar Planet. Sci.* **36**, #1750 (abstr.).

Kita N. T., Ushikubo T., Kimura M., Nyquist L. E. and Valley J. W. (2008) Heterogeneous oxygen isotope ratios of olivine in chondrules from Y-793408 (H3.2) chondrite. *Meteorit. Planet. Sci. Suppl.* **43**, A77.

Kita N. T., Ushikubo T., Fu B. and Valley J. W. (2009a) High precision SIMS oxygen isotope analysis and the effect of sample topography. *Chem. Geol.* **264**, 43–57.

Kita N. T., Goodrich C. A., Spicuzza M. J. and Valley J. W. (2009b) Oxygen isotopes in ungrouped achondrite NWA 1500 and comparison to brachinites. *Lunar Planet. Sci.* **40**, #1393 (abstr.).

Kobayashi S., Imai H. and Yurimoto H. (2003) New extreme $_{16}O$-rich reservoir in the early solar system. *Geochem. J.* **37**, 663–669.

Krot A. N., Zolensky M. E., Wasson J. T., Scott E. R. D., Keil K. and Ohsumi K. (1997) Carbide-magnetite-bearing type 3 ordinary chondrites. *Geochim. Cosmochim. Acta* **61**, 219–237.

Krot A. N., Libourel G., Goodrich C. A. and Petaev M. I. (2004) Silica-rich igneous rims around magnesian chondrules in CR carbonaceous chondrites: evidence for condensation origin from fractionated nebular gas. *Meteorit. Planet. Sci.* **39**, 1931–1955.

Krot A. N., Yurimoto H., McKeegan K. D., Leshin L., Chaussidon M., Libourel G., Yoshitake M., Huss G. R., Guan Y. B. and Zanda B. (2006) Oxygen isotopic compositions of chondrules: implications for evolution of oxygen isotopic reservoirs in the inner solar nebula. *Chem. Erde* **66**, 249–276.

Krot A. N., Amelin Y., Bland P., Ciesla F. J., Connelly J., Davis A. M., Huss G. R., Hutcheon I. D., Makide K., Nagashima K., Nyquist L. E., Russell S. S., Scott E. R. D., Thrane K., Yurimoto H. and Yin Q.-Z. (2009) Origin and chronology of chondritic components: a review. *Geochim. Cosmochim. Acta* **73**, 4996–4997.

Krot A. N., Nagashima K., Ciesla F. J., Meyer B. S., Hutcheon I. D., Davis A. M., Huss G. R. and Scott E. R. D. (2010) Oxygen isotopic composition of the sun and mean oxygen isotopic composition of the protosolar silicate dust: evidence from refractory inclusions. *Astrophys. J.* **713**, 1159–1166.

Kunihiro T., Rubin A. E., McKeegan K. D. and Wasson J. T. (2004) Oxygen-isotopic compositions of relict and host grains in chondrules in the Yamato 81020 CO3.0 chondrite. *Geochim. Cosmochim. Acta* **68**, 3599–3606.

Kunihiro T., Rubin A. E. and Wasson J. T. (2005) Oxygen-isotopic compositions of low-FeO relicts in high-FeO host chondrules in Acfer 094, a type 3.0 carbonaceous chondrite closely related to CM. *Geochim. Cosmochim. Acta* **69**, 3831–3840.

Kurahashi E., Kita N. T., Nagahara H. and Morishita Y. (2008) ^{26}Al–^{26}Mg systematics of chondrules in a primitive CO chondrite. *Geochim. Cosmochim. Acta* **72**, 3865–3882.

Lewis R. D., Lofgren G. E., Franzen H. F. and Windom K. E. (1993) The effect of Na vapor on the Na content of chondrules. *Meteoritics* **28**, 622–628.

Libourel G., Krot A. N. and Tissandier L. (2006) Role of gas–melt interaction during chondrule formation. *Earth Planet. Sci. Lett.* **251**, 232–240.

Libourel G. and Krot A. N. (2007) Evidence for the presence of planetesimal material among the precursors of magnesian chondrules of nebular origin. *Earth Planet. Sci. Lett.* **254**, 1–8.

Lyons J. R. and Young E. D. (2005) CO self-shielding as the origin of oxygen isotope anomalies in the early solar nebula. *Nature* **435**, 317–320.

Makide K., Nagashima K., Krot A. N., Huss G. R., Hutcheon I. D. and Bischoff A. (2009) Oxygen- and magnesium-isotope compositions of calcium–aluminum-rich inclusions from CR2 carbonaceous chondrites. *Geochim. Cosmochim. Acta* **73**, 5018–5050.

Maruyama S., Yurimoto H. and Sueno S. (1999) Oxygen isotope evidence regarding the formation of spinel-bearing chondrules. *Earth Planet. Sci. Lett.* **169**, 165–171.

Maruyama S. and Yurimoto H. (2003) Relationship among O, Mg isotopes and the petrography of two spinel-bearing compound chondrules. *Geochim. Cosmochim. Acta* **67**, 3943–3957.

Mayeda T. K., Clayton R. N. and Sodonis A. (1989) Internal oxygen isotope variations in 2 unequilibrated chondrites. *Meteoritics* **24**, 301.

McKeegan K. D., Leshin L. A., Russell S. S. and MacPherson G. J. (1998) Oxygen isotopic abundances in calcium–aluminum-rich inclusions from ordinary chondrites: implications for nebular heterogeneity. *Science* **280**, 414–418.

McKeegan K. D., Kallio A. P. A., Heber V. S., Jarzebinski G., Mao P. H., Coath C. D., Kunihiro T., Wiens R., Alltonm J. and Burnett D. S. (2010) Genesis SiC Concentrator sample traverse: confirmation of 16O-depletion of terrestrial oxygen. *Lunar Planet. Sci.* **41**, #2589 (abstr.).

Mostefaoui S., Kita N. T., Togashi S., Tachibana S., Nagahara H. and Morishita Y. (2002) The relative formation ages of ferromagnesian chondrules inferred from their initial aluminum-26/aluminum-27 ratios. *Meteorit. Planet. Sci.* **37**, 421–438.

Nagahara H., Kushiro I. and Mysen B. O. (1994) Evaporation of olivine – low-pressure phase-relations of the olivine system and its implication for the origin of chondritic components in the solar nebula. *Geochim. Cosmochim. Acta* **58**, 1951–1963.

Nagahara H., Ozawa K. and Tomomura S. (2005) Kinetic condensation of silicate melt and its role in the chemical diversity of chondrules. In *Chondrites and the Protoplanetary Disk*, vol. 341 (eds. A. N. Krot, E. R. Scott and B. Reipurth). Astronomical Society of the Pacific Conference Series, pp. 456–468.

Nagahara H., Kita N. T., Ozawa K. and Morishita Y. (2008) Condensation of major elements during chondrule formation and its implication to the origin of chondrules. *Geochim. Cosmochim. Acta* **72**, 1442–1465.

Nakamura T., Noguchi T., Tsuchiyama A., Ushikubo T., Kita N. T., Valley J. W., Zolensky M. E., Kakazu Y., Sakamoto K., Mashio E., Uesugi K. and Nakano T. (2008) Chondrule-like objects in short-period comet 81P/Wild 2. *Science* **321**, 1664–1667.

Onuma N., Clayton R. N. and Mayeda T. K. (1972) Oxygen isotope cosmothermometer. *Geochim. Cosmochim. Acta* **36**, 169–188.

Pack A., Yurimoto H. and Palme H. (2004) Petrographic and oxygen-isotopic study of refractory forsterites from R-chondrite Dar al Gani 013 (R3.5–6), unequilibrated ordinary and carbonaceous chondrites. *Geochim. Cosmochim. Acta* **68**, 1135–1157.

Richet P., Bottinga Y. and Javoy M. (1977) Review of hydrogen, carbon, nitrogen, oxygen, sulfur, and chlorine stable isotope fractionation among gaseous molecules. *Annu. Rev. Earth Planet. Sci.* **5**, 65–110.

Richter F. M. (2004) Timescales determining the degree of kinetic isotope fractionation by evaporation and condensation. *Geochim. Cosmochim. Acta* **68**, 4971–4992.

Russell S. S., MacPherson G. J., Leshin L. A. and McKeegan K. D. (2000) O-16 enrichments in aluminum-rich chondrules from ordinary chondrites. *Earth Planet. Sci. Lett.* **184**, 57–74.

Sakamoto N., Seto Y., Itoh S., Kuramoto K., Fujino K., Nagashima K., Krot A. N. and Yurimoto H. (2007) Remnants of the early solar system water enriched in heavy oxygen isotopes. *Science* **317**, 231–233.

Tachibana S. and Huss G. R. (2005) Sulfur isotope composition of putative primary troilite in chondrules from Bishunpur and Semarkona. *Geochim. Cosmochim. Acta* **69**, 3075–3097.

Tachibana S., Nagahara H., Mostefaoui S. and Kita N. T. (2003) Correlation between relative ages inferred from Al-26 and bulk compositions of ferromagnesian chondrules in least equilibrated ordinary chondrites. *Meteorit. Planet. Sci.* **38**, 939–962.

Thiemens M. H. and Heidenreich J. E. (1983) The mass-independent fractionation of oxygen – a novel isotope effect and its possible cosmochemical implications. *Science* **219**, 1073–1076.

Tissandier L., Libourel G. and Robert F. (2002) Gas–melt interactions and their bearings on chondrule formation. *Meteorit. Planet. Sci.* **37**, 1377–1389.

Tomomura S., Nagahara H., Tachibana S., Kita N. T. and Morishita Y. (2004) Relationship between bulk chemical composition and formation age of chondrules in Bishunpur and Krymka. *Lunar Planet. Sci.* **35**, #1555 (abstr.).

Ushikubo T., Kimura M., Kita N. T. and Valley J. W. (2009) Oxygen isotopic compositions of phenocrysts in chondrules from the primitive carbonaceous chondrite Acfer 094. *Lunar Planet. Sci.* **40**, #1383 (abstr.).

Valley J. W. and Kita N. (2009) In situ oxygen isotope geochemistry by ion microprobe. In *Mineralogical Association of Canada Short Course*, vol. 41, Toronto, pp. 19–63.

Valley J. W., Kitchen N., Kohn M. J., Niendorf C. R. and Spicuzza M. J. (1995) UWG-2, a garnet standard for oxygen isotope ratios: strategies for high precision and accuracy with laser heating. *Geochim. Cosmochim. Acta* **59**, 5223–5231.

Wang J., Davis A. M., Clayton R. N., Mayeda T. K. and Hashimoto A. (2001) Chemical and isotopic fractionation during the evaporation of the $FeO–MgO–SiO_2–CaO–Al_2O_3–TiO_2$ rare earth element melt system. *Geochim. Cosmochim. Acta* **65**, 479–494.

Yoneda S. and Grossman L. (1995) Condensation of $CaO–MgO–Al_2O_3–SiO_2$ liquids from cosmic gases. *Geochim. Cosmochim. Acta* **59**, 3413–3444.

Young E. D. and Russell S. S. (1998) Oxygen reservoirs in the early solar nebula inferred from an Allende CAI. *Science* **282**, 452–455.

Yu Y., Hewins R. H., Clayton R. N. and Mayeda T. K. (1995) Experimental-study of high-temperature oxygen-isotope exchange during chondrule formation. *Geochim. Cosmochim. Acta* **59**, 2095–2104.

Yu Y., Hewins R. H., Alexander C. M. O. and Wang J. (2003) Experimental study of evaporation and isotopic mass fractionation of potassium in silicate melts. *Geochim. Cosmochim. Acta* **67**, 773–786.

Yurimoto H. and Wasson J. T. (2002) Extremely rapid cooling of a carbonaceous-chondrite chondrule containing very ^{16}O-rich

olivine and a ^{26}Mg-excess. *Geochim. Cosmochim. Acta* **66**, 4355–4363.

Yurimoto H. and Kuramoto K. (2004) Molecular cloud origin for the oxygen isotope heterogeneity in the solar system. *Science* **305**, 1763–1766.

Zhao Z. F. and Zheng Y. F. (2003) Calculation of oxygen isotope fractionation in magmatic rocks. *Chem. Geol.* **193**, 59–80.

Associate editor: Alexander N. Krot